

Department of Physics and Astronomy

University of Heidelberg

Master thesis

in Physics

submitted by

Martin Fleck

2014

**Commissioning a gas chromatograph for automatic
measurements of gas compositions in the ALICE
TPC and TRD**

and

**Measurement of electrons from semi-leptonic
heavy-flavour hadron decays in p-Pb collisions at
 $\sqrt{s_{\text{NN}}} = 5.02 \text{ TeV}$ with the ALICE TRD**

This Master thesis has been carried out by Martin Fleck

at the

Physikalisches Institut Heidelberg

under the supervision of

Dr. rer. nat., Priv.-Doz. Kai Schweda

Commissioning a gas chromatograph for automatic measurements of gas compositions in the ALICE TPC and TRD and Measurement of electrons from semi-leptonic heavy-flavour hadron decays in p-Pb collisions at $\sqrt{s_{\text{NN}}} = 5.02$ TeV with the ALICE TRD

Abstract

The gas mixture of a gas detector affects its drift velocity and gas gain and therefore the precise knowledge of the gas composition is crucial for detector calibration, online monitoring and trigger generation. For this purpose, a gas chromatography system that automatically provides measurements of the gas composition in the ALICE TPC and TRD has been set up and implemented in the respective detector control system for graphical display and archiving of the measurement results and for their immediate use in calibration procedures. Before suppression effects that are seen in Pb-Pb collisions can be regarded as a property of the quark-gluon plasma, proton-nucleus collisions must be studied in order to identify non-QGP nuclear effects. For this purpose the ALICE TPC and TRD were used to measure the nuclear modification factor R_{pPb} of electrons from heavy-flavour hadron decays in minimum bias events for a pseudorapidity $|\eta| < 0.5$ at $\sqrt{s_{\text{NN}}} = 5.02$ TeV. The resulting nuclear modification factor is compatible with unity in the measured transverse momentum range from 2 GeV/c to 12 GeV/c, indicating that the suppression seen in Pb-Pb collisions is due to the final state of the system.

Zusammenfassung

Das Gas eines Gasdetektors beeinflusst dessen Driftgeschwindigkeit und Gasverstärkung. Die Zusammensetzung des Gases ist für die Kalibration und Überwachung des Detektors sowie für die Triggergenerierung von großer Bedeutung. Zu diesem Zweck wurde ein Gaschromatographiesystem in Betrieb genommen, das automatisch die Gaszusammensetzung im TRD und der TPC des ALICE Experiments misst. Weiterhin wurde der Gaschromatograph ins Detektorkontrollsystem eingebunden, womit archivierte und aktuelle Messergebnisse als Funktion der Zeit graphisch dargestellt werden können und das deren Verwendung in weiterführenden Kalibrationen ermöglicht.

Wenn in Pb-Pb Kollisionen abweichende Ergebnisse zur pp Physik gemessen werden, können diese Effekte nicht ohne Weiteres als Einfluss des Quark-Gluon-Plasmas aufgefasst werden, weswegen in Proton-Blei-Kollisionen jene Effekte erforscht werden, die auf die Eigenschaften des Bleikerns zurückzuführen sind. Dazu wurde mit der Kombination von TPC und TRD PID der nukleare Modifikationsfaktor R_{pPb} bei einer Schwerpunktsenergie von $\sqrt{s_{\text{NN}}} = 5.02$ TeV für semileptonische Zerfälle von schweren Quarks im Pseudorapiditätsbereich $|\eta| < 0.5$ gemessen. Im transversalen Impulsbereich von 2 GeV/c bis 12 GeV/c ist R_{pPb} kompatibel mit 1, so dass die in Pb-Pb Kollisionen gemessenen Effekte auf den Endzustand der Pb-Pb Kollision zurückzuführen sind.

Contents

1. Introduction to ALICE and motivation	1
1.1. ALICE Time Projection Chamber	2
1.2. ALICE Transition Radiation Detector	2
1.3. Gas and gas system of the ALICE TRD	6
1.3.1. Overview on the TRD gas system	7
1.4. TPC gas and gas system of the ALICE TPC	8
I. Commissioning a gas chromatograph for automatic measurements of gas compositions in the ALICE TPC and TRD	11
2. Gas chromatography and gas chromatograph	13
2.1. Functionality and features of the Chromatograph	14
2.1.1. The columns	15
2.1.2. The oven	17
2.1.3. The stream selector	18
2.1.4. The sampling loop and the sampling process	18
2.1.5. The carrier gas	19
2.1.6. The thermal conductivity detector	21
2.2. Description Agilent ChemStation “methods”	21
2.2.1. The two-stage separation process	22
2.3. Run automation	24
2.4. Peak identification	24
2.5. Precision of gas composition measurements	25
3. DIM and WinCC-OA	27
3.1. Data read out and transport	28
3.2. WinCC panel	30
3.3. Setup Stability	30
4. Calibration	33
4.1. Absolute calibration	33
4.2. Automated relative calibration	34
5. Maintenance	37

6. Summary and prospects	39
II. Measurement of electrons from semi-leptonic heavy-flavour hadron decays in p-Pb collisions at $\sqrt{s_{\text{NN}}} = 5.02$ TeV with the ALICE TRD	41
7. Motivation	43
8. Introduction	45
8.1. Outline of the analysis	45
8.2. Dataset and Monte Carlo simulation	45
8.3. Event Selection	46
8.4. Track selection	46
9. Particle identification	49
10. Efficiency and efficiency correction	55
10.1. Refining the implementation of the TRD in the Monte Carlo simulation	55
10.2. Validation for using Monte Carlo efficiency correction	58
10.3. Monte Carlo efficiency correction	64
10.3.1. Efficiency correction with only TRD tracking enabled	64
10.3.2. Efficiency with TRD tracking and TRD particle identification	67
11. Estimation of systematic uncertainties	71
12. Results: HFE spectrum and R_{pPb}	75
12.1. Summary and prospects	78
Appendix	80
A. Miscellaneous practical information for setting up the chromatograph	83
A.1. Enable XML file export of Agilent ChemStation	83
A.2. Pre-run parameters - auxillary commands	83
A.3. Setting up Visual Studio to compile a DIM server	84
A.4. Miscellaneous hints	84
B. Tables	85
C. Lists	87
Bibliography	97

1. Introduction to ALICE and motivation

ALICE[1] is A Large Ion Collider Experiment at the CERN LHC. It is a general-purpose heavy-ion detector, optimized to study the quark-gluon plasma (QGP) and the strong interaction at extreme temperature and/or particle density that occur in ultra-relativistic nucleus-nucleus collisions at the LHC.

In quantum chromodynamics (QCD), the potential V between a quark anti-quark pair in vacuum contains a term that increases linearly with distance:

$$V(r) = -\frac{\alpha}{r} + kr \tag{1.1}$$

Because of this feature, it is energetically preferred to produce a new quark anti-quark pair when separating a quark from its anti-quark partner. Thus, quarks can not be observed as single free particles, but occur only in bound states called hadrons. This phenomenon is called confinement.

At extreme temperatures, the coupling between QCD color charges in the quark-gluon plasma becomes weak and quarks experience asymptotic freedom, as if there was no confinement (“deconfinement”). Matter in the early universe is believed to have existed as a quark-gluon plasma.

The physics goal of ALICE requires the detector to be able to deal with the extremely large particle multiplicities that are expected in Pb-Pb collisions at LHC energies and to provide particle identification over a broad momentum range, including the low momentum regime.

The main device for tracking and particle identification in the central barrel of the ALICE experiment is the time projection chamber (TPC). Its particle identification properties are complemented by measurements of further detectors. For example, electron particle identification can be extended towards low momenta with the time of flight detector (TOF).

With increasing momentum it is more and more difficult to distinguish electrons from hadron tracks (especially pions that are produced in abundance) in the TPC signal. The transition radiation detector addresses this challenge, by providing a measurement of transition radiation, which in a wide momentum range is only produced for the light electron and thus allows to distinguish high momentum electron tracks from hadron tracks.

1.1. ALICE Time Projection Chamber

The main apparatus for tracking and particle identification in the central barrel of the detector is the ALICE TPC (fig. 1.1), a gaseous time-projection chamber. Its structure is a hollow cylinder of 88 m^3 whose axis coincides with the LHC beam-pipe (z -axis of the global ALICE coordinate system). Between the central high voltage electrode and the readout chambers (fig. 1.2), a uniform electric field is applied. Parallel to this drift field is the magnetic field of the L3 magnet.

Charged particles passing the drift volume of the TPC ionize the medium along their track and electrons from the ionization process drift towards the readout planes, located at either sides of the cylinder. The location of a track in the plane orthogonal to the beam pipe is obtained directly from the position of a signal on the readout plane. The position of a track in z is inferred from arrival time and signal amplitude and thus a 3D image of tracks can be reconstructed. The arrival time is directly proportional to the drift velocity of electrons in the TPC medium. The drift velocity is a function of the applied electric and magnetic fields and further depends on the density and on the composition c of the gas mixture [2]. The gas density ρ is a function of pressure, temperature and gas composition c . Thus the drift velocity is

$$v_d = v_d(E, B, \rho(P, T, c), c). \quad (1.2)$$

Increasing the nitrogen concentration in the TPC gas mixture from 0% to 10% at a constant drift field of $E/p = 1\text{ V cm}^{-1}\text{ mbar}^{-1}$, results in a 15% change in the drift velocity [3]. Likewise, the amplification factor of the signal at the anode wires in the TPC (gas gain) is affected by the gas composition: An addition of nitrogen to the TPC gas mixture similar to the above, requires a change of the anode voltage from 1.4 kV to 1.6 kV in order to obtain a similar gas gain value [3]. The dependency of v_d on the gas composition is one of the motivating reasons to analyse the gas composition with a gas chromatograph. Precise knowledge of the gas composition is valuable information for accurate drift velocity predictions.

1.2. ALICE Transition Radiation Detector

The Transition Radiation Detector (TRD, fig. 1.1) of ALICE is a tracking detector with triggering capabilities specifically designed for electron identification.

The TRD exploits the phenomenon of transition radiation to identify electrons. When a relativistic charged particle passes a boundary between two media of different dielectric constants, there is a probability of emitting a photon. The average energy of this transition radiation (TR) photon is approximately proportional to its Lorentz factor γ [4]. In practice, a critical value of

$$(\beta\gamma)_{\text{crit}} \approx \gamma_{\text{crit}} = 1000 \quad (1.3)$$

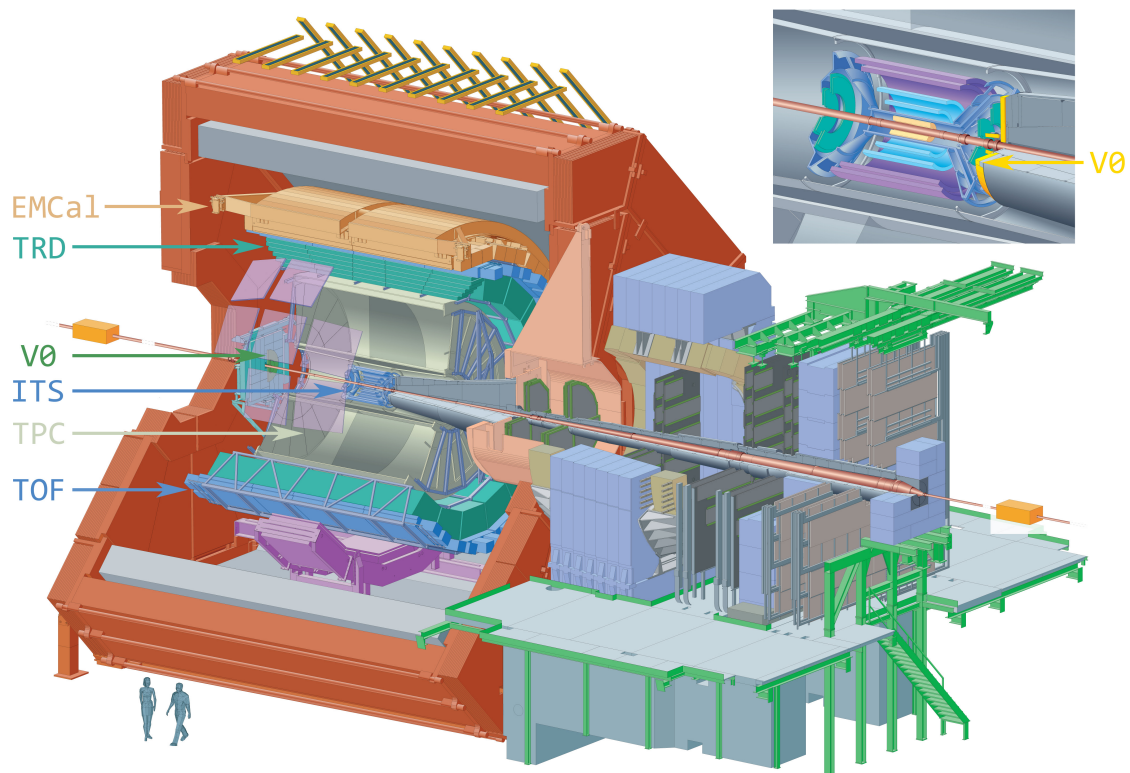


Figure 1.1.: A schematic view of ALICE [1]. The detectors that are relevant for this thesis have been labeled.

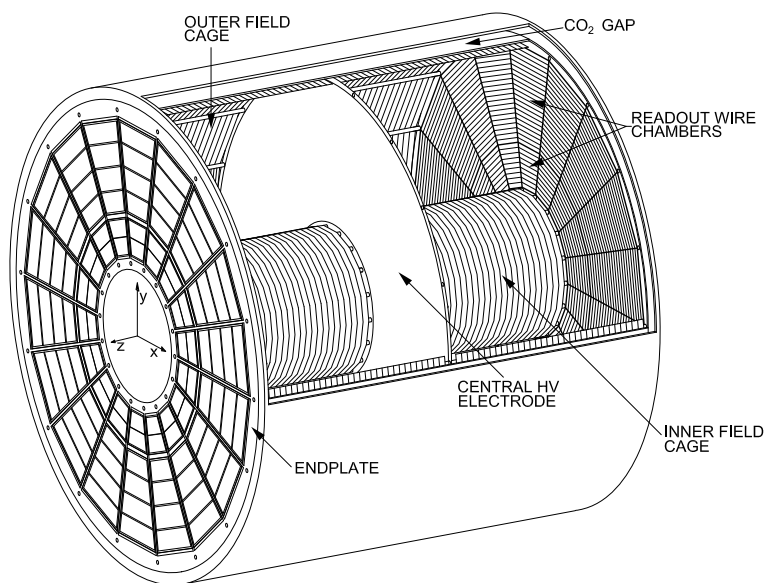


Figure 1.2.: A schematic view of the ALICE TPC [2].

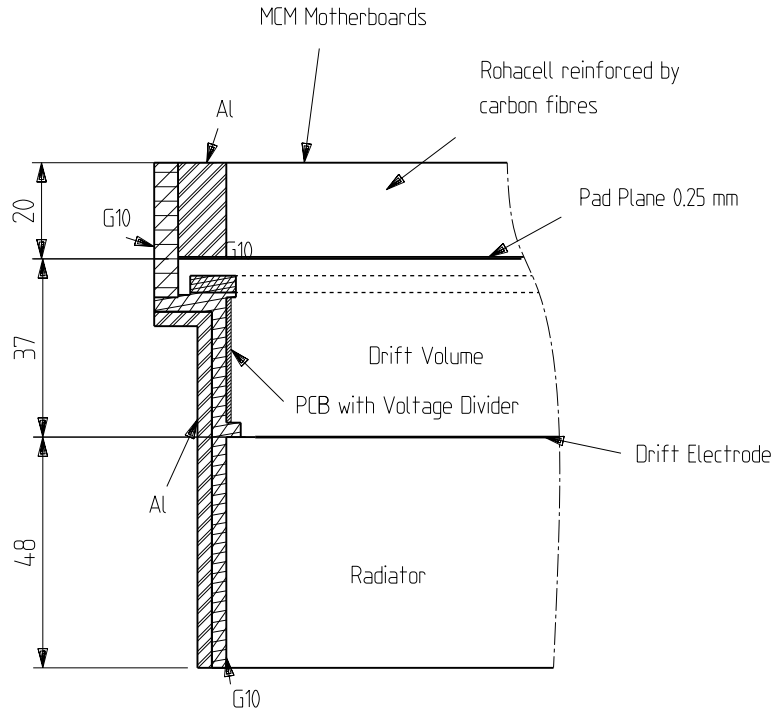


Figure 1.3.: Cross section through a TRD detector module [5]. The dimensions are given in mm, e.g the drift volume has a depth of 37 mm. Particles pass from bottom to top.

is necessary to produce a detectable TR photon [4] (natural units are used). The momentum of a particle of mass m depends on $\beta\gamma$:

$$p = (\beta\gamma) \cdot m \quad (1.4)$$

resulting in a critical momentum of electrons of $p_e \approx 0.5 \text{ GeV}$ and $p_\pi \approx 140 \text{ GeV}$ for pions, leaving a wide momentum window for electron identification.

A TRD module (fig. 1.3) consists of a multiwire proportional readout chamber together with a radiator, in which electrons can produce a TR photon. Charged particles passing the drift chamber ionize the gas. An electric field applied between an electrode on top of the radiator and a plane of cathode wires on the opposite side of the drift volume drifts the electrons from ionization towards the wire plane. A further plane of thin anode wires provides gas amplification: In the electric field close to the wire, ionization electrons are accelerated and gain enough energy to in turn ionize the surrounding medium. In this way, an avalanche is created, that amplifies the track signal such that the current is strong enough to induce a charge on the pad plane, where the readout electronics is located. As for the TPC, gas gain is influenced by the gas composition, as e.g. the average energy that is required to produce an ion pair depends, amongst other things, on the type of gas [6]. Every single TRD module is a fully functional detector unit and a high-energy particle propagating through the TRD is measured individually in each chamber that is intersected by the trajectory of the track. The part of a track

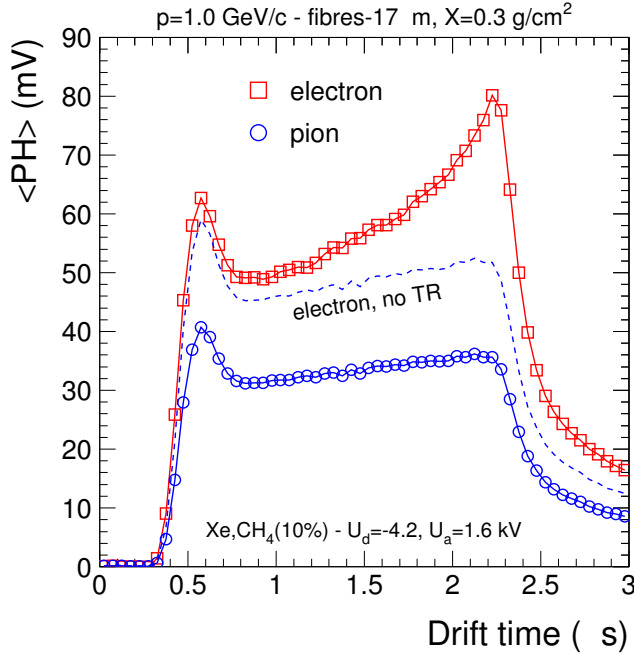


Figure 1.4.: Mean pulse height of the signal of an electron and pion track induced on the pad plane, as a function of drift time [5].

that is measured in a single chamber of the TRD is called a tracklet. A signal from a single tracklet has a certain length in time of about the maximum drift length towards the wires divided by the drift velocity. The ALICE TRD can read out the signal of a tracklet as a function of (drift-)time. For this purpose, the signal of a tracklet is divided into seven time bins (called “slices”), allowing the characteristic time dependence of TR photon absorption to be used for particle identification with the TRD. The detector gas is chosen for maximum absorption cross section of the radiators transition radiation. Consequently, if a TR photon is present, the characteristic increase of the signal pulse height is seen at high drift times (fig. 1.4). In this way, not only the additional charge after TR photon absorption, but also characteristics of the absorption mechanism are exploited in order to optimize electron identification. Additionally, energy loss of electrons in gas is higher in general, compared to other particles.

These phenomena make it possible to distinguish electrons from other particles. The influence of the gas composition on drift velocity and thus drift time (equation 1.2) and the importance of drift time and gas gain for the TRD measurement principle motivate the chromatographic analysis of the gas composition.

The complete ALICE TRD will consist of 522 of these chambers that are arranged into 18 super modules aligned in a cylinder to cover the complete azimuth. Each super module is split in z direction into five stacks of which each consists of six layers of chambers that are stacked in radial direction. In the three super modules

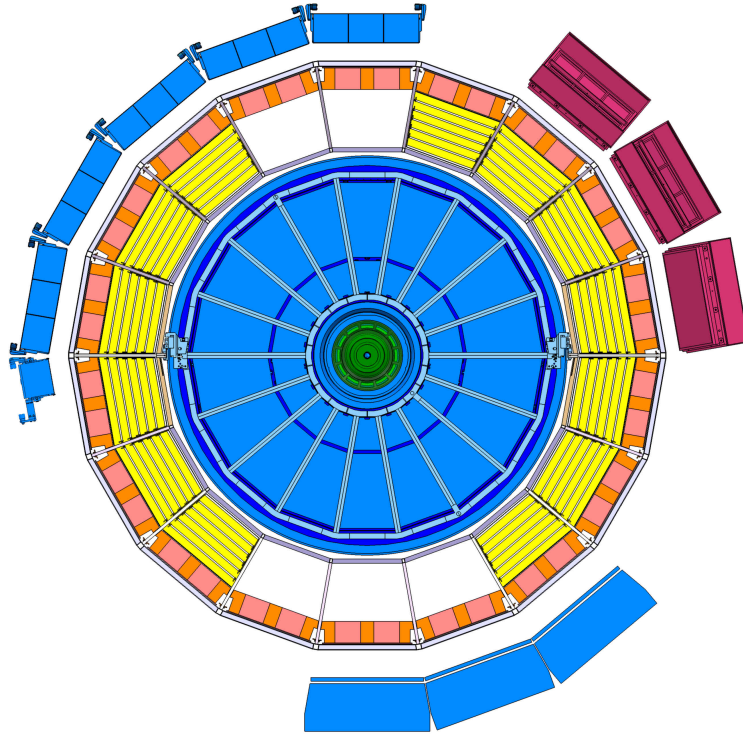


Figure 1.5.: ALICE cross section, indicating the installation status of the TRD during the 2013 data runs.

that cover the same azimuth as the ALICE photon spectrometer (PHOS, blue structure at the bottom of fig. 1.5) the middle stacks contain no chambers in order to reduce the material budget for PHOS. During the 2013 p-Pb runs, during which the data was taken that is used in the analysis presented in the second part of this thesis, not all super modules of the TRD have been installed in ALICE. The installation status of the detector at that time is depicted in fig. 1.5.

1.3. Gas and gas system of the ALICE TRD

As gas is the detecting medium of both the TRD and the TPC, the type of gas mixture is of vital importance for the performance of the detector. Typical gas mixtures involve a noble gas and a quencher gas. The gas provides ionization electrons from passing high energy particles. When an ionized atom or molecule of the detector gas recombines with an electron, the electron may be in an excited state and emit a photon to enter its ground state. The quencher absorbs the photons from this processes through excitation of vibrational and rotational modes, which otherwise could liberate an electron from the various electrodes in a detector and produce a signal. The addition of CO_2 to a pure noble gas mixture also drastically increases electron drift velocity at low electric fields[7], so that viable drift velocities are attained.

For the TRD a gas mixture[5] of 85% Xe and 15% CO_2 is used. Xenon fulfills

the requirement for a large absorption cross section for the TR photon. As xenon is costly, a closed gas system is required. CO₂ is cheap, easy to handle (non-flammable) and has adequate quencher performance. For hydrogen-containing molecules, high-energy particles can free a proton from the molecule that in turn can produce a signal of its own (“knock-on proton”). The CO₂ molecule does not contain hydrogen, so background from knock-on protons is not an issue.

1.3.1. Overview on the TRD gas system

An overview of the basic features of a gas detector gas system shall be given, using the example of the TRD gas system. The basic task of the gas system is to provide and circulate the reference gas mixture and to keep the pressure in the detector ≤ 1 mbar above atmospheric pressure. The location of the different units of the TRD gas system is depicted in fig. 1.6 [5]. A general layout of the TRD gas system is shown in fig. 1.7 [5].

The returning gas from the detector flows through 18 return lines (one for each super module). At the outlet of each super module, a pressure sensor is installed that is linked with a control valve at the return lines and thus regulates the overpressure of ≤ 1 mbar in the super modules. Thus the gas has very little overpressure at the return lines. To make gas circulation possible, a compressor is installed at this stage in order to increase the pressure. After compression, the gas is pumped into a buffer unit that can accept and release gas, compensating for the varying amount of gas in the system that is needed to keep a constant overpressure in the super modules when ambient pressure is changing.

Following the buffer, the gas is pumped to the surface gas building (SG2) where a purifier system is installed that can remove oxygen and water contaminations due to leaks. However, the purifier can not remove nitrogen from the system. Nitrogen enters the gas system through leaks. No gas system is perfectly gas tight and the low volume-to-surface ratio of the TRD (the width of the TRD drift volume in radial direction is only 3.7cm (fig. 1.3)) is an unfavourable influence on gas tightness in particular. The removal of nitrogen is handled by a cryogenic recovery system that can separate nitrogen from the Xe-CO₂ mixture and remove it from the system.

Filling of the gas system with the reference mixture, e.g. after a shut-down period when the detector modules are flushed with CO₂, is achieved by the mixer unit. Filling as well as circulation is carried out in a closed loop circulation mode. The mixer unit can regulate the flow according to the desired fraction of each gas component in the mixture. For the removal of CO₂ (which is necessary during filling and done before the recovery process), a set of semi-permeable membranes is installed that utilize the different permeability through a porous material due to different molecular size to separate CO₂ (small molecule size) from xenon (large molecule size) [8]. During the filling process the membranes are used to remove superfluous purging gas (CO₂) from the system as it is continuously replaced by xenon until the reference composition is attained.

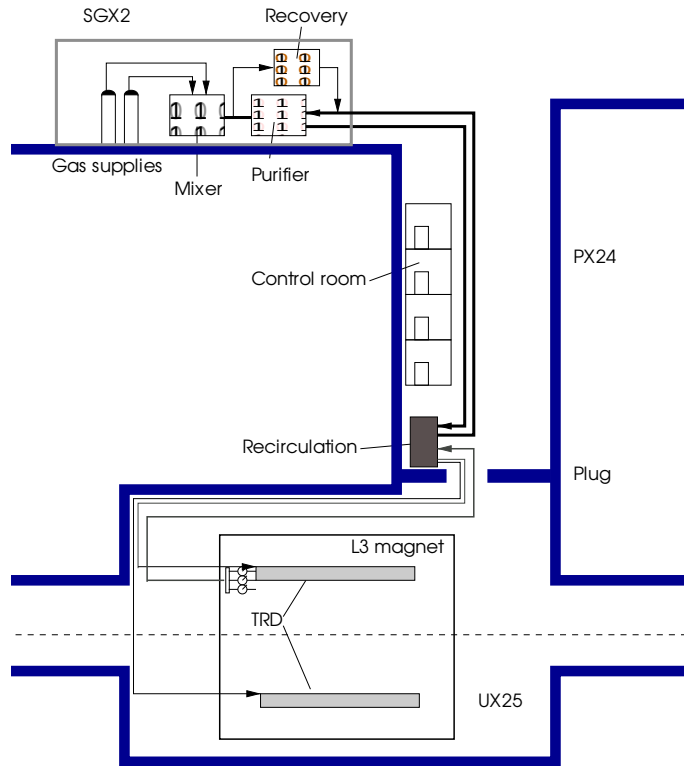


Figure 1.6.: Locations of the various units of the TRD gas system [5].

Following the membranes and the mixer unit at the surface, the gas returns underground to the plug (fig. 1.6) and is distributed to the TRD super modules at appropriate pressure and flow.

The gas chromatograph is connected to the TRD gas system with two inlet connections, one before and one after the purifier unit in the surface gas building SG2.

1.4. TPC gas and gas system of the ALICE TPC

Many factors play a role in choosing suited gas for a TPC that needs to perform in heavy-ion and p-p runs at high collision rates [7]. Because of the large drift volume, a high electron drift velocity is required to minimize dead time. Again due to the huge drift lengths, gases of low density and thus low radiation length are preferred to reduce the material budget and thus multiple scattering. Electron diffusion has negative influence on spatial resolution and thus on momentum resolution of the TPC. These are some of the most important requirements from the physics point of view.

Non-flammable gases are strongly preferred in order to avoid expensive safety measures. The current gas mixture for operation consists of 90% argon, 10% CO₂.

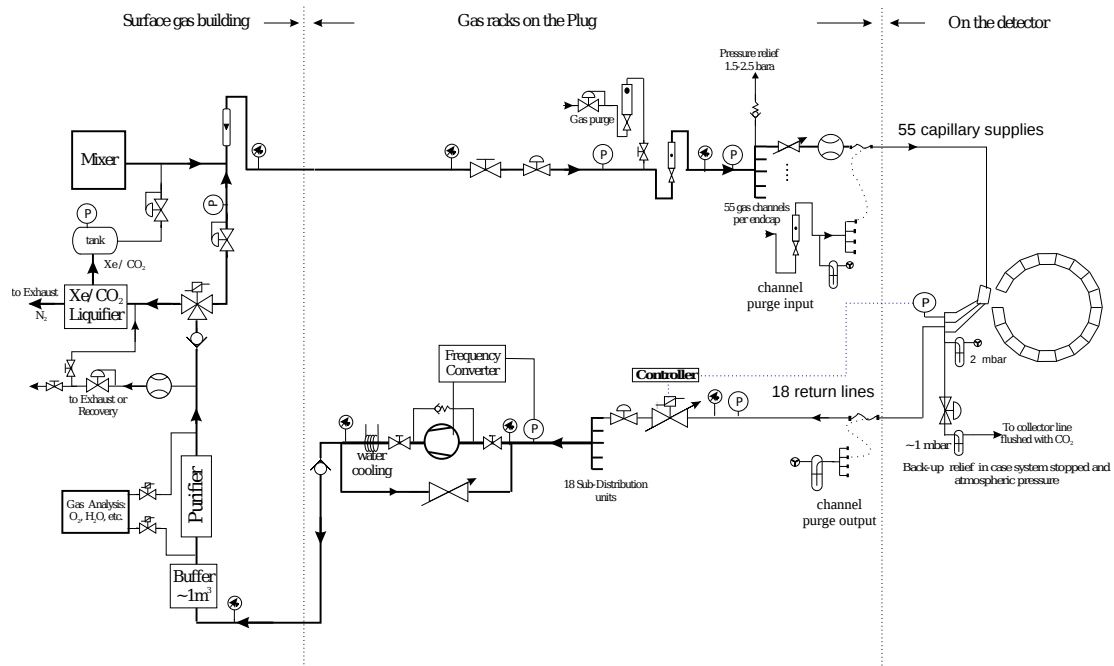


Figure 1.7.: General layout of the TRD gas system [5]. (The position of the buffer unit is not in the surface gas building, as depicted here, but on the plug.)

The gas system shall not be discussed in detail. The basic structure of the gas system is resembling that of the TRD, i.e. mixer unit, purifier and pump and pressure regulation are installed in a similar fashion.

Part I.

Commissioning a gas chromatograph for automatic measurements of gas compositions in the ALICE TPC and TRD

2. Gas chromatography and gas chromatograph

The term “chromatography” denotes a process of separating mixtures. In order to measure the composition of a gas mixture, first it needs to be separated and then detection of the amount of every individual component can happen.

In gas chromatography, separation is achieved by pushing the gas mixture through a thin and long tube, the column. The interaction strength of each gas component with a special coating on the inner walls¹ of the column (the stationary phase) determines the amount of time that each compound needs to pass through a column. This time, the retention time t_R , is specific to the component which allows for identification of compounds.

The retention time is the sum of two contributions:

$$t_R = t_M + t'_R, \quad (2.1)$$

with the hold-up time t_M that it takes a compound which only stays in the mobile phase to pass the column and the adjusted retention time t'_R , the time that a compound stays in the stationary phase and does not move along the column. Factors that determine t'_R are the vapor pressure of a compound and intermolecular forces [9] e.g. due to non-zero dipole moment or non-zero partial charges of a molecule.

The adjusted retention time and the hold up time are linked to the volumes of stationary and mobile phase [9], V_S and V_M , via the distribution constant K_i that is characteristic for a substance as well as for the stationary phase material:

$$\frac{t'_R}{t_M} = K_i \frac{V_S}{V_M} \quad (2.2)$$

Depending on their distribution constant K_i , different substances will exit the column after different amounts of time and are thus separated. After a mixture is separated, the amount of each compound is (in this application) measured with a thermal conductivity detector (TCD).

¹ Historically it was found that separation strength strongly depends on uniformity of the stationary phase. This led to the conclusion to substitute the many different microscopic paths through a filled column with one single way: A coated tube with a consistent opening in its center (“capillary column”). The higher permeability achieved in this way allows for longer column lengths, increasing resolution for a given stationary phase [9].

2.1. Functionality and features of the Chromatograph

A gas chromatograph (GC) is a device that is able to perform the above mentioned steps of separation and detection on gaseous compounds. A tremendous benefit of using chromatography for measuring gas compositions is the versatility of this approach, which makes it possible to quantitatively analyse a wide variety of gas mixtures, including but not limited to mixtures of argon, xenon, neon, CO₂, nitrogen and oxygen that are relevant for the operation of the ALICE TPC and TRD.

Needed for basic operation of a gas chromatograph are:

- An injector that introduces the sample gas into the chromatograph,
- one or more columns, that supply the stationary phase for separation,
- flow of carrier gas that, among other tasks, together with the sample gas constitutes the mobile phase,
- temperature and pressure regulation that adjust the column temperature and carrier gas pressure to ascertain repeatable separation conditions and
- a detector, measuring the quantity of each substance exiting the column.

The area of a peak that is registered by the detector is proportional to the amount of the corresponding substance. This is the principal link to obtain a quantitative result on the composition of a gas mixture. In modern chromatography systems, an essential part of the chromatograph is the software with which it is controlled that, among other things, is responsible for the integration of the peak areas.

The chromatograph that is used is an Agilent 7890A gas chromatograph [10] (fig. 2.1). Additional components are a stream selector and switching valves, that were assembled by SRA Instruments [11]. A schematic flow diagram of the very chromatograph that is used is given in fig. 2.3. The combination of stream selector, sampling loop and valve 1 (V1) performs the function of an injector.

The measurement output of a successful analysis is called a chromatogram. An example chromatogram, showing the result of an analysis of the TPC gas is shown in fig. 2.2. The signal of the TCD (in units of 25 μ V) is plotted as a function of time. The peak at a retention time of 3 minutes corresponds to CO₂, the peak at 5.9 minutes to argon. At 5.5 minutes a peak of neon with a relative area of 0.009% (uncalibrated) is present as a remainder from the previously used gas mixture in the TPC. The peak at 2.8 minutes is a measurement artifact that is produced when the switching valve V2 is actuated. The peak 7.5 minutes is of unknown origin.

Two software packages are provided for controlling the gas chromatograph. In principle, the chromatograph is controlled using Agilent ChemStation [12]. However the stream selector by SRA Instruments can not be used by ChemStation and therefore a further software is needed. SRA provides SRA ProChem [13] that can exercise control over the stream selector and act as supervision software for Agilent



Figure 2.1.: The Agilent 7890A gas chromatograph (a) with the stream selector (b) and switching valves (c) by SRA.

ChemStation.

In practice, the parameters for the chromatographic analysis are set up and stored as methods in Agilent ChemStation and run time control is handled by SRA ProChem.

In the following subsections, the relevant features of this chromatography system and their functionality are described.

2.1.1. The columns

The separation process is influenced by the column parameters, which are

- type of stationary phase,
- inner diameter of a capillary column,
- column length and
- film thickness (compare eq. 2.2).

By far the strongest influence on the separation process is due to the type of the stationary phase [9]. For some mixtures it is not possible to achieve separation using only one type of stationary phase. This is the case if e.g. additional to the current TPC gas mixture of CO₂ and argon, contaminations of nitrogen are

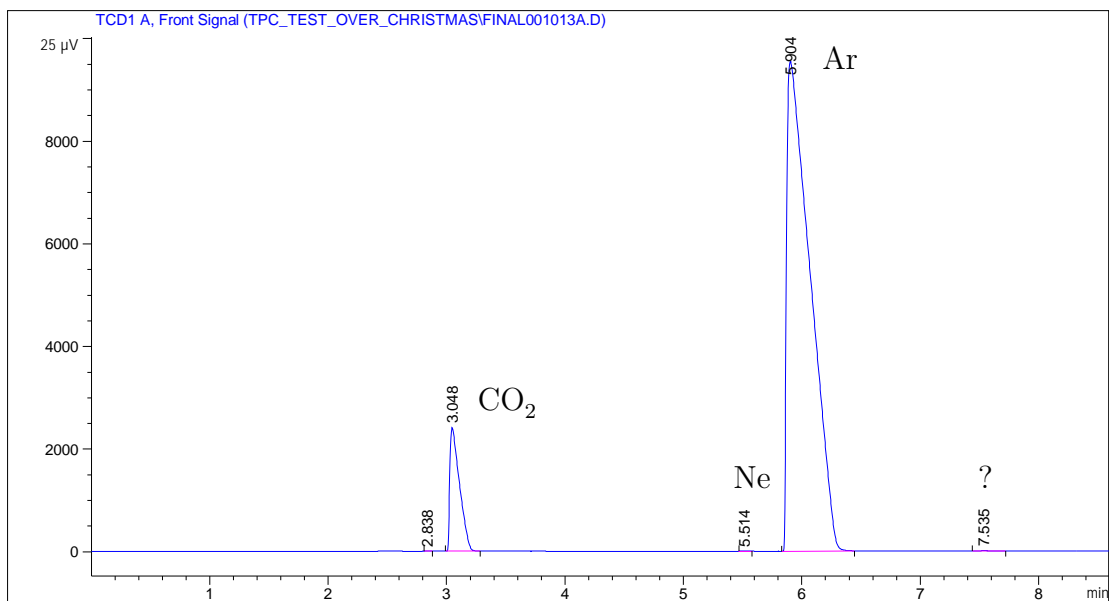


Figure 2.2.: A chromatogram for the TPC gas as produced by Agilent ChemStation. Vertical numbers denote the retention time in minutes of any peak that the software found. Magenta parts of the time axis illustrate the region that was used for integration of peak area. The peak at a retention time of 3 minutes corresponds to CO₂, the peak at 5.9 minutes to argon. At 5.5 minutes a peak of neon with a relative area of 0.009% (uncalibrated) is present as a remainder from the previously used gas mixture in the TPC. The peak at 2.8 minutes is a measurement artifact that is produced when the switching valve V2 is actuated. The peak 7.5 minutes is of unknown origin.

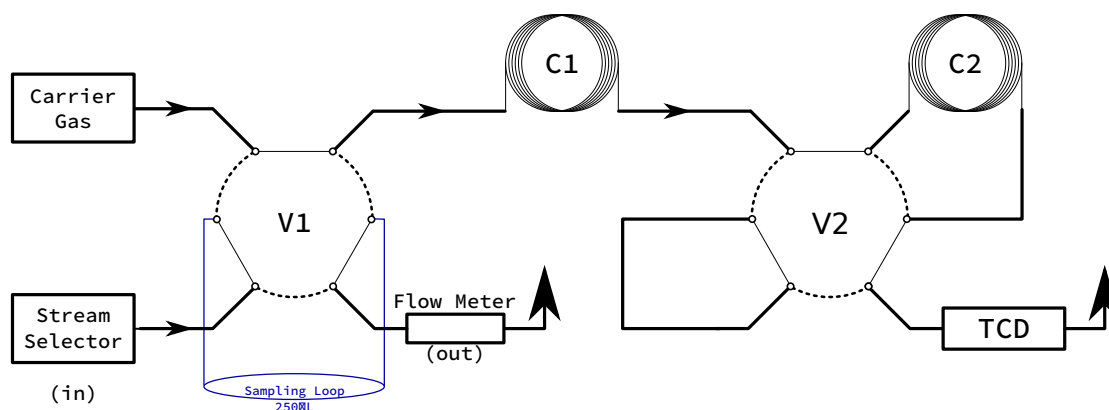


Figure 2.3.: Schematic, depicting the switching valve layout of the gas chromatograph. The compounds being analysed enter the system at the stream selector. The switching valves V1 and V2 have two states (on/off). The dashed (thin) lines show the interconnections that the valves use in the “on”(“off”) state. For example, if V1 is on and V2 off, the carrier gas pushes the content of the sampling loop through Column 1 and 2 (C1 and C2) to the TCD and the outlet of the Stream Selector is directly exhausted through a flow meter.

present.

In this chromatographic application, this issue is resolved via a two-stage separation of CO_2 . Therefore the chromatograph features two columns that are connected in series. The first stage can separate CO_2 from all other gases. The second column can further separate the CO_2 -free gas mixture. Additionally, the second column absorbs CO_2 . It is coated with a molecular sieve: A material with holes of uniform size, such that CO_2 molecules are trapped but Ar, Xe and N_2 pass unhindered. The steps to achieve separation of the TPC and TRD gas mixtures are explained in 2.2.1. The columns that are used have a diameter of $535\ \mu\text{m}$ and a film thickness of $50\ \mu\text{m}$. Column 1 is 25 m and column 2 is 30 m long.

2.1.2. The oven

Gas chromatographic separation can be done on substances that can be evaporated (without dissociating), in which case the analysis has to be carried out at a temperature higher than the highest boiling temperature of all substances involved. Besides, the width of the peaks exiting the column and the retention times are influenced by the temperature of the gas and the column during the separation process. Substances that have a low boiling point (as it is the case in this application) show higher peak width with increasing temperature. For both reasons, to avoid condensation and to ascertain repeatable separation conditions, the columns are located in a heatable chamber, the oven. In this application, only gaseous compounds are analysed. Consequently, the oven is operated at $40\ ^\circ\text{C}$,

Stream number	Gas source
1	TPC
2	TPC calibration gas
3	spare 1
4	TRD purifier in
5	TRD purifier out
6	TRD calibration gas
7	Membranes
8	TRD Recovery
9	spare 2
10	compressed air

Table 2.1.: Connection layout of the stream selector. On the software side, there is an eleventh stream (“default stream”) that is selected in order to close an open stream.

as low as possible in order to maximize separation efficiency, but high enough to be independent of high ambient temperatures in summer. The oven is capable of reaching temperatures up to 450 °C. If a mixture contains compounds with a large variety of boiling temperatures (and thus very different vapor pressure values) it can be useful to ramp the oven temperature during an analysis in order to combine good separation and reasonable peak width for all compounds.

2.1.3. The stream selector

The chromatograph is required to analyse samples from multiple sources, e.g. gas from the TPC and from the TRD gas systems as well as calibration gas mixtures with TPC and TRD gas composition. For this purpose, there are then selectable electrovalves at the inlet of the gas chromatograph, from which one can be selected for analysis at runtime. This part of the chromatograph is called the stream selector. A list of the current connection layout of the stream selector is given in tab. 2.1.

2.1.4. The sampling loop and the sampling process

To obtain a sample of defined size from the gas mixture, a loop with a volume of 50 μL , the sampling loop, is filled with the gas mixture that shall be analysed. A loop is an apt way to obtain high-purity gas samples of fixed volume. By simply flushing the total volume of the loop for several times until sufficient purity is reached, a sample is prepared (“sampling”).

A second loop with a volume of 250 μL is available for installation. However, with

the larger sample size, the peaks of xenon and CO₂ of the TRD gas are not fully separated but have a small overlap, which is not the case when the smaller sampling loop is used (fig. 2.4). With a smaller sampling volume, the absolute peak size decreases. Separation in time, however, is unchanged and close peaks are separated better.

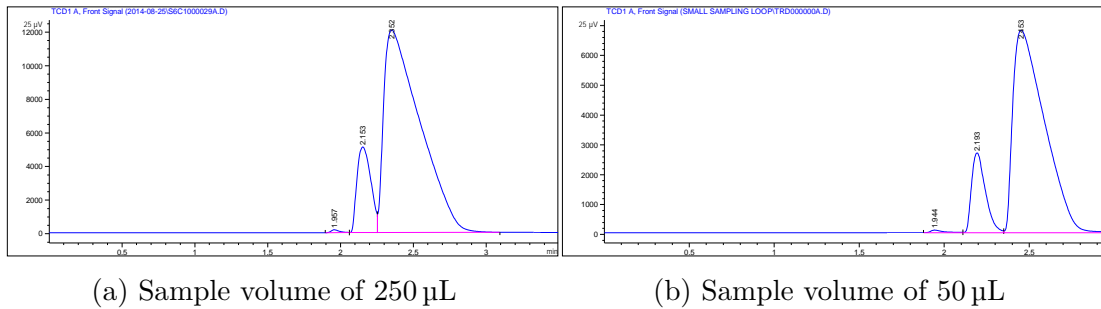


Figure 2.4.: Analysis of the TRD gas using two sampling loops of different size. The three peaks from left to right correspond to air, CO₂ and xenon. The smaller sampling volume (b) visibly improves separation of Xenon and CO₂. The air that is present in this measurements is contamination in the tubing that connects the chromatograph and the TRD calibration gas tank and presumably entered the system during the installation of this connection.

For analysis, the content of the sampling loop needs to enter the chromatograph. A switching valve (V1, fig. 2.3) can connect the sampling loop either to the stream selector (for sampling) or to the columns for separation and subsequent analysis by the TCD.

During sampling, V1 is off, and the sampling loop is connected to the stream selector and to the outlet at the flow meter, purging the loop with sampling gas while the columns are exposed to a flow of carrier gas only. At run time, V1 is switched on and the sampling loop is connected to the carrier gas flow and to the columns. The sample in the loop is pushed through the columns by the carrier gas. After V1 is on, the sample gas inlet at the stream selector is closed.

2.1.5. The carrier gas

It is the flow of carrier gas that pushes the sample through the columns. Thus carrier gas pressure and flow directly influences retention times and peak shapes. Helium is used as carrier gas. It is further used as reference gas for the TCD and to actuate the pneumatic switching valves V1 and V2.

In order to not disturb the chromatographic process and to minimize detector noise, it is crucial that high purity gas (> 99.999%) is used [9]. Because of similar pricing, helium of purity $\geq 99.9999\%$ has been used so far.

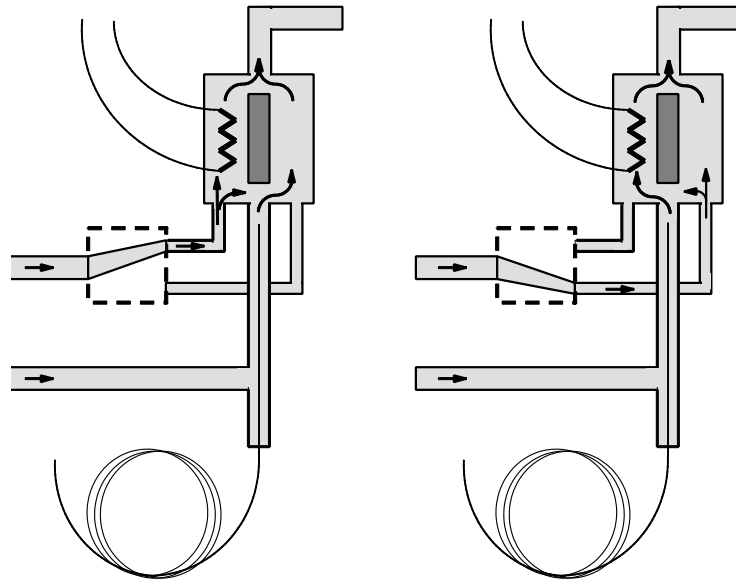


Figure 2.5.: Schematic drawing of the TCD [14]. From the bottom upwards, the effluent of the columns is mixed with the make-up gas before it reaches the chamber where the filament (zigzag structure) is located. A switching valve (dashed box) can be set to push the column effluent away from (or towards) the filament as shown in the left (right) diagram, such that reference gas (or sampling gas from the columns) flows over the filament. The filament is heated and when it is in alternating contact with gases of different thermal conductivity, its temperature (and thus its resistance) changes. The resistance change is measured in a wheatstone bridge circuit that produces the TCD output signal. The switching valve is set to operate at 5Hz.

2.1.6. The thermal conductivity detector

The thermal conductivity detector (TCD) compares the thermal conductivity of the output flow from the columns with a reference flow of pure carrier gas (fig. 2.5 [14]). The detector consists of a heated filament that is in alternating contact with the carrier gas and with the effluent from the columns. Gaseous compounds (with the exception of hydrogen) generally have a lower thermal conductivity than helium. When such a compound comes into contact with the filament, the heat flow from the filament is decreased and its temperature rises, which can be measured as an increase in its resistance. In order to measure the small changes in voltage drop over a resistor, the filaments are arranged in a wheatstone bridge circuit. Accordingly the output signal of the TCD is in volts.

For temperatures below 150 °C the filament is not turned on [14]. In order to maximize sensitivity and filament lifetime it is recommended [15] to use the lowest possible temperature to operate the TCD. The minimum temperature must be higher than the highest boiling point of the measured compounds so that no condensation can happen. A further limiting case can be if hydrogen is measured with helium as carrier gas: Hydrogen is the only element that has a higher thermal conductivity than helium. However mixtures of helium and up to 20% of hydrogen result in thermal conductivities that are less than each compound on its own, which results in unpredictable peak polarity of hydrogen peaks. This problem can be solved by using high TCD temperature settings of 200 °C to 300 °C [14]. As no hydrogen and only gaseous compounds are analysed, the limit for a viable temperature is not restricted further. It was decided to keep the temperature at 170 °C, which is still low but well above the hardware limit.

Between the exit of the column and the entry to the TCD (compare fig. 2.5), a further gas inlet of (in this application) helium is installed to increase the flow through the detector. This is referred to as make-up gas. Its main purpose is to induce a faster transition of the peaks through the detector in order to prevent remixing of separated peaks at the detecting stage.

2.2. Description Agilent ChemStation “methods”

“Method” is the term that is used in chromatography to denote the set of all parameters that is used to perform an analysis of a single sample with the GC. The most important settings to be stored in a method are

- carrier gas flow and pressure,
- oven temperature setting,
- TCD temperature and make-up gas flow values and
- timing and initial position of switching valve actuation.

Carrier gas pressure and oven temperature setting can be ramped in order to deal with mixtures of substances exhibiting a wide variety of retention times or a wide range of boiling temperatures.

Parameters that influence the way in which peak integration is performed can also be varied for each method. This becomes important, when two peaks are not separated completely and have a certain overlap. In this case, the baseline that is used for integration can be adapted in order to improve repeatability of the integration results.

A crucial aspect for a successful analysis is the initial position of each of the two pneumatic valves and the appropriate time to actuate the valves in order to accomplish the two-stage separation of CO₂ from the mixture.

In the following paragraph the procedure to separate all components of the gas mixtures used in the TPC and TRD is explained.

2.2.1. The two-stage separation process

The separation process is explained using the example of the TPC gas mixture. TRD gas separation can be done using the very same procedure as for the TPC gas. The few minute difference are explained hereafter.

For a mixture of argon, CO₂ and nitrogen, it is not possible to achieve separation using only one type of stationary phase. In this application, two different columns are used to achieve separation of all components. Using only column 1 for separation results in a chromatogram as is shown in fig. 2.6. Column 1 separates a mixture of e.g. Ar, Ne, N₂, O₂, and CO₂ into two peaks: One containing CO₂ (the smaller peak in fig. 2.6) and the other containing all the other compounds (in this example, the peak contains mainly argon and a trace amount of neon from the gas mixture previously used in the TPC). In column 2 the latter peak can be further separated into its individual components. However, column 2 absorbs CO₂. Thus, a complete analysis must execute the following steps:

1. Filling of the sampling loop (sampling). The initial position of valve 1 is therefore required to be off (compare fig. 2.3).
2. Switch on valve 1. This pushes the content of the sampling loop to column 1, separating CO₂ from the other components. The peak that requires further separation in column 2 exits column 1 before CO₂ (compare fig. 2.6), therefore the initial position of valve 2 is required to be off.
3. Switch on valve 2 before CO₂ goes into column 2. This leads CO₂ directly to the TCD, bypassing column 2. During that time, there is no flow through column 2. The compounds are stored.
4. Switch off valve 2 after CO₂ is detected in the TCD, resuming flow and separation of the compounds in column 2.

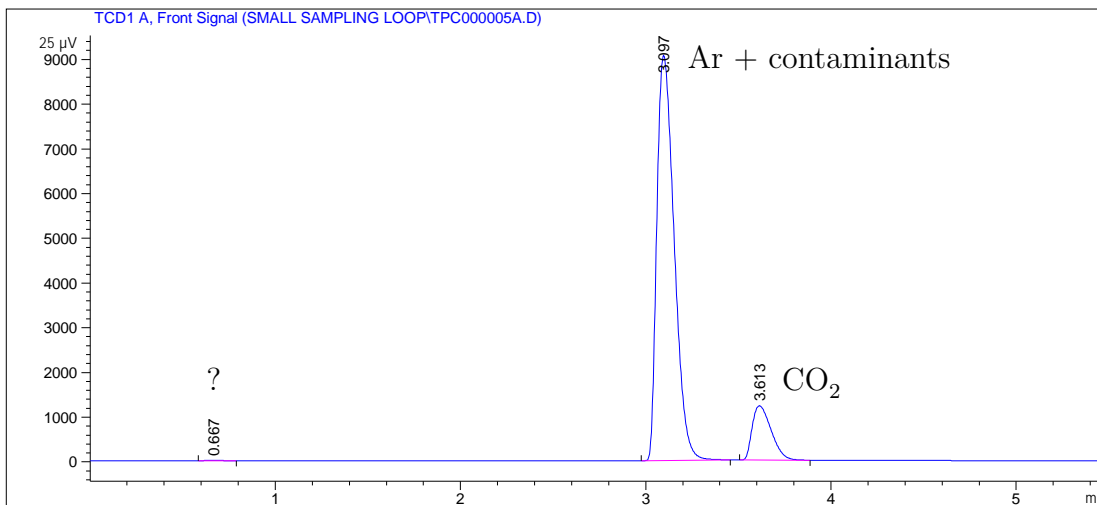


Figure 2.6.: Analysis of the TPC gas, using only column 1 for separation.

Using this series of operations on a gas mixture, all components but CO₂ undergo a second separation in column 2 that allows for individual detection of all components, including CO₂, in the TCD. In fig. 2.2 on page 16 a full separation of the TPC gas using all of the above steps is shown. Compared to the separation using only column 1 (fig. 2.6) the total measurement time increases, as the argon-containing peak has to pass through the second column before detection and the argon-containing peak is further separated into a pure argon peak and a neon peak. Possible nitrogen contaminations would be visible at this stage at a retention time of circa 8 minutes.

The determination of the right switching times to actuate the valve in step 4 can be tricky. The exact time can not be read from the chromatograms, as an unknown amount of time passes between a substance exiting the column and its detection in the TCD. The chromatograms provide an educated guess as a starting point from which the right switching time can be obtained by incrementing in small steps, using trial and error.

The xenon in the TRD gas mixture is different in that it is already present as an isolated peak after using column 1 only (fig 2.7). The only change to the above steps needed for a successful analysis is that a longer wait is required until step 4 can be performed, as xenon requires more time than CO₂ to pass column 1.

When only one type of contamination is expected (e.g. nitrogen), an analysis using only column 1 is sufficient to measure the purity of the gas mixture. This simpler measurement procedure has the advantage to be less prone to error (e.g. unknowingly cutting peak tails when switching the valve in step 4). It further shortens the analysis time, which, however, is not real benefit in this application. However, the nature of the contamination is only verified, when column 2 is used in the analysis. Therefore, the full analysis using both columns is preferred.

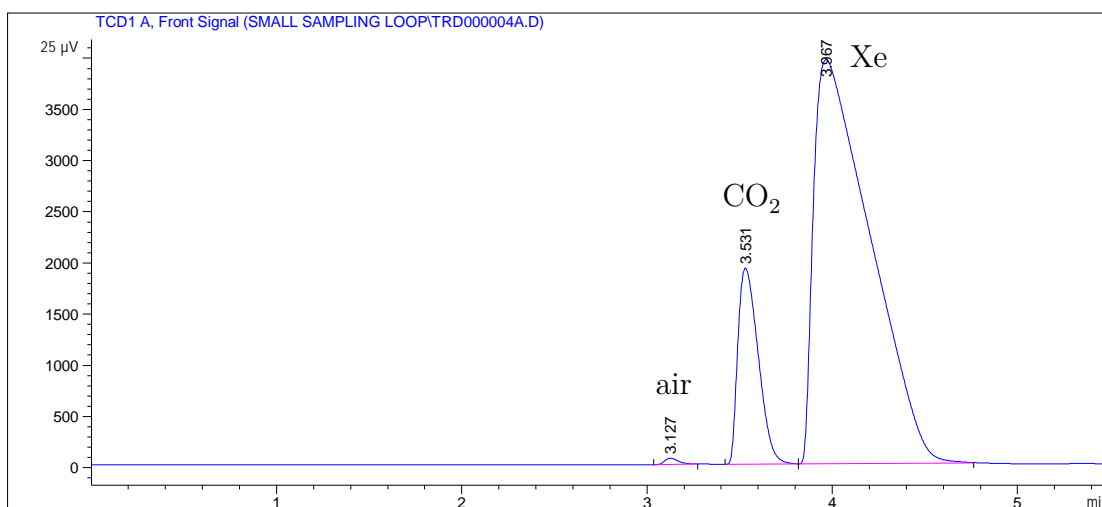


Figure 2.7.: Analysis of the TRD gas, using only column 1 for separation.

2.3. Run automation

An individual analysis is performed, running the gas chromatograph with a certain method. Several methods can be grouped into a sequence of methods using e.g. SRA ProChem. Optionally, either fixed waiting periods between each method of a sequence can be set in SRA ProChem or arbitrary pauses can be introduced, using methods that do no analysis (but e.g. reduce carrier gas and make-up gas flow to reduce helium consumption). A sequence can be repeated continuously, thus providing an automated measurement on all required input streams over any desired period in time.

2.4. Peak identification

From a chromatogram like fig. 2.2 it can be read how many compounds make up the gas mixture. However, further information is needed to associate a peak with a certain substance. Only when the retention time of a substance is known, a peak can be identified with a specific compound such as argon or nitrogen. As the TPC and TRD gas are simple gas mixtures with only two components, peak identification is straight forward. As the gas composition is known to be similar to the reference mixture, the peaks of the main compounds can be identified directly via the relative peak area (the larger peak is xenon (argon) in the TRD (TPC) gas).

A further method is to identify CO_2 by its presence in both mixtures: Using only column 1 for separation (and keeping all run parameters constant), the peak of CO_2 in the TPC gas can be found at the same retention time as in the TRD gas. Additionally, CO_2 is absorbed in column 2 and thus can be identified.

In order to determine the retention times of nitrogen and oxygen, a gas bottle of

compressed air is available. Similar to the above, both can be distinguished by the difference in their peak size. However, in a sample of pure air the peaks of nitrogen and oxygen are large and thus broad. A small peak, e.g. as it is expected to occur due to nitrogen contamination in the detector gas, does not necessarily show up at the same retention time where the maximum of a very large peak is located. In order to improve peak identification and reduce detection artefacts for small peaks, it is preferable to determine the retention times from peaks of small size.

In order to produce small nitrogen (and oxygen) peaks, a small quantity of air can be introduced into the system, by disconnecting the input stream (switching to the default stream) some seconds before starting the analysis. This can be achieved when the auxiliary commands of SRA ProChem (see appendix A.2) are intentionally set up in an improper order. In this way the retention time of a N_2 whose size is comparable with that of a contamination can be determined.

2.5. Precision of gas composition measurements

In order to estimate the precision with which the gas composition can be determined, the TPC gas was measured repeatedly for a month-long period of time. The distribution of the uncalibrated relative peak area values (fig. 2.8) shows a multi-peak structure and strong correlation between the measurements of the two gas components.

It was observed, that the measured values of the gas composition are correlated with the pressure with which the gas enters the sampling loop, which is determined by the pressure in the buffer unit of the detector gas system that is turn anticorrelated to the ambient pressure: The pressure in the detector must be close to ambient pressure and therefore the buffer must release gas into (accept gas from) the system when ambient pressure rises (drops). The multi peak structure is due to the various ambient pressure conditions during this measurement period. If a change in pressure causes an increase of the volume fraction of one of the gas components, the volume fraction of the other component decreases, hence the correlation of both histograms.

In this study, the fraction of each component of the TPC gas mixture could be measured with a precision of $\pm 0.014\%$ (fig. 2.8). This value, however, depends on the pressure changes in the environment. A similar test that was made at an earlier time resulted in a measurement precision of the gas fraction of $\pm 0.041\%$. To what extent this results can be transferred to measurements of small peaks of contaminations is still to be determined.

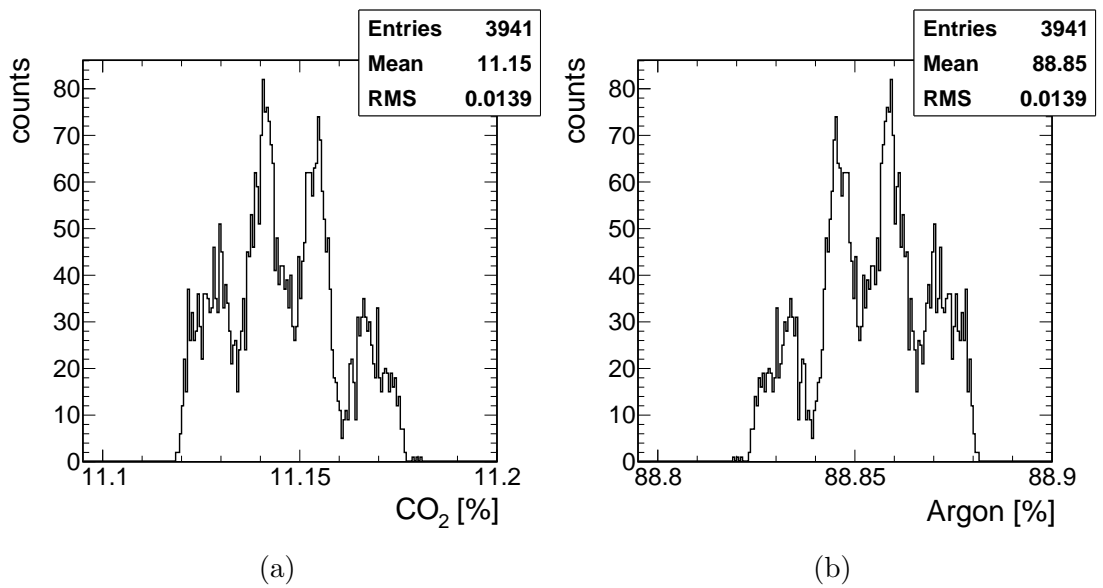


Figure 2.8.: Histograms, showing the distributions of the measured CO₂ (a) and argon (b) fraction in the TPC gas that were obtained over the period of one month of continuous measurements.

3. DIM and WinCC-OA

The value of the chromatography system that we want to establish lies in automation and data reduction. The details of chromatography and the handling of the machine and software is a means to obtain information on the gas composition. Only this more abstract information is relevant information for the performance of the detector.

The control over the vast number of electronics that is required to operate the experiments at the LHC is brought together in a Supervisory Control And Data Acquisition (SCADA) system. The purpose of such a system is to be able to monitor and provide detailed (low level) and abstract (high level) control over the operation of a vast number of different machinery and electronics from within a single piece of software. The chromatography system presented here was included in the ALICE SCADA system, the detector control system (DCS). The tool that the Joint Controls Project chose to build the SCADA system with which the LHC and its experiments are controlled is called WinCC-OA.

There are several ways how WinCC-OA can communicate with various hardware devices. An industry standard that is widely used for this purpose is called “OLE for Process Control” (OPC). Many companies offer OPC servers for control and readout of their hardware. Agilent, however, does not offer an OPC server for their 7890A gas chromatograph. In principal, the functionality of an OPC server can be written from scratch, if an application programming interfaces that manages communication with the hardware is available. In this case the communication with WinCC can be handled by the DIM protocol (Distributed Information Management System) [16] that was written and released by CERN under the GNU General Public License. However, this procedure is neither officially supported nor documented by Agilent.

Controlling the gas chromatograph from within WinCC, for which direct communication with e.g. an OPC sever is required, is not a priority (if at all reasonable). Important is that the obtained gas composition values are transfered to WinCC for display and archiving. Thus, a sufficient solution is to let the software store the measurement results and subsequently read out these data files. The DIM protocol can be used for communication of this data to WinCC. A DIM server that provides this functionality was written in the course of this thesis.

3.1. Data read out and transport

A convenient and flexible way to obtain structured measurement result data from the Agilent 7890A is to enable XML output (described in appendix A.1). The XML files hold all information that can be obtained from a chromatogram (retention time, peak are, peak height for each peak) but not the chromatogram itself. Additional meta-information such as injection time and date, stream number, name of the method that was used and information like software and firmware version number, etc. is stored as well.

For each measurement, Agilent ChemStation creates a new folder with a unique name where the XML file (“Result.xml”) is stored. As long as a measurement is in progress, there is a file named “ACQUIRING.txt” that contains the folder name of the next measurement. The process that contains the DIM server waits for the creation of either file and reads out their content.

A DIM server is a process that is able to provide information (e.g. integers, floats or strings but also complex data types are possible) in form of DIM services to DIM clients. There are several types of services available in the DIM protocol. The type of service that is used for the DIM server of the gas chromatograph is a “monitored” service, which means that the client is updated when the service information changes (e.g. after a new chromatographic analysis of the TRD gas, the relative content of xenon is updated).

An important link between client and server is the DIM name service (DNS). Clients request services (identified by a unique service name) from the DNS and servers declare or register the list of services they can provide to the DNS. If a service is registered with the DNS and a client request this very service, the DNS shares the network location of the client with the server and vice versa. Server and client will then continue to communicate directly with one another.

When a DIM server crashes or is shut down, the clients that subscribed to services of this server stay idle. As soon as the server is back online and registers itself with the DNS, the clients are again provided with updated services. Migration of a DIM server to a different machine, with a different network address, is thus only a matter of stopping the DIM server on the old machine and starting it on the new machine.

Besides the read out of data from the XML file that stores the measurement results, the process containing the DIM server is also used for peak identification based on retention time. For each analysis, the DIM server process carries out the following steps:

- Wait for the file “ACQUIRING.txt” to be created.
- From this file, read the folder name of the ongoing measurement.
- Wait for the XML file to be created that folder.
- Get the stream number (compare tab. 2.1) from the XML file and decide if the data belongs to the TPC or TRD WinCC control system.

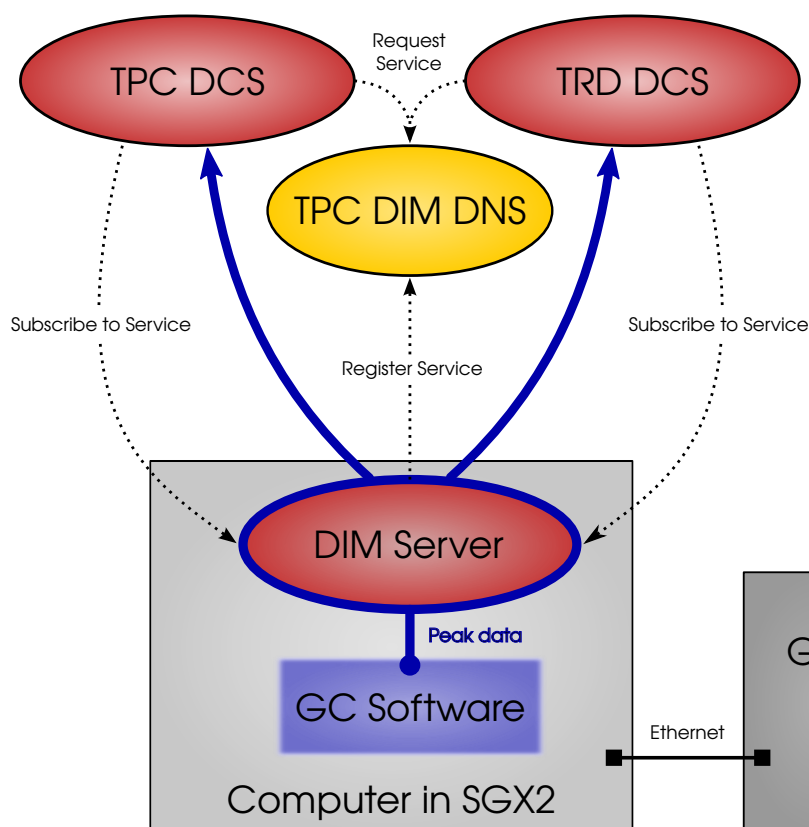


Figure 3.1.: Illustration of the data flow from the gas chromatograph to the detector control systems of the TPC and TRD.

- Loop over all peaks: Get the retention time and area of each peak. If there is a peak with known retention time and reasonable peak area, update the according DIM service with its relative peak area. For example, it can be requested that the CO_2 peak in the TRD gas will only be identified as such when it is above a reasonable threshold value. Possible small peaks (artifacts, noise) can be ruled out this way without a downside, since in operation mode, the CO_2 fraction will never be significantly below 15%.

A layout depicting the structure of data transport between the detector control system of the TPC and TRD and the machine on which the software of the gas chromatograph is running, is given in fig. 3.1. Both the TRD and TPC DCS use the same DIM name server (DNS). Every DIM service has a unique name that contains the compound name that was measured and that identifies it as belonging to either the TPC or TRD. The DIM clients of the TPC and TRD DCS only subscribe to TPC or TRD services respectively.

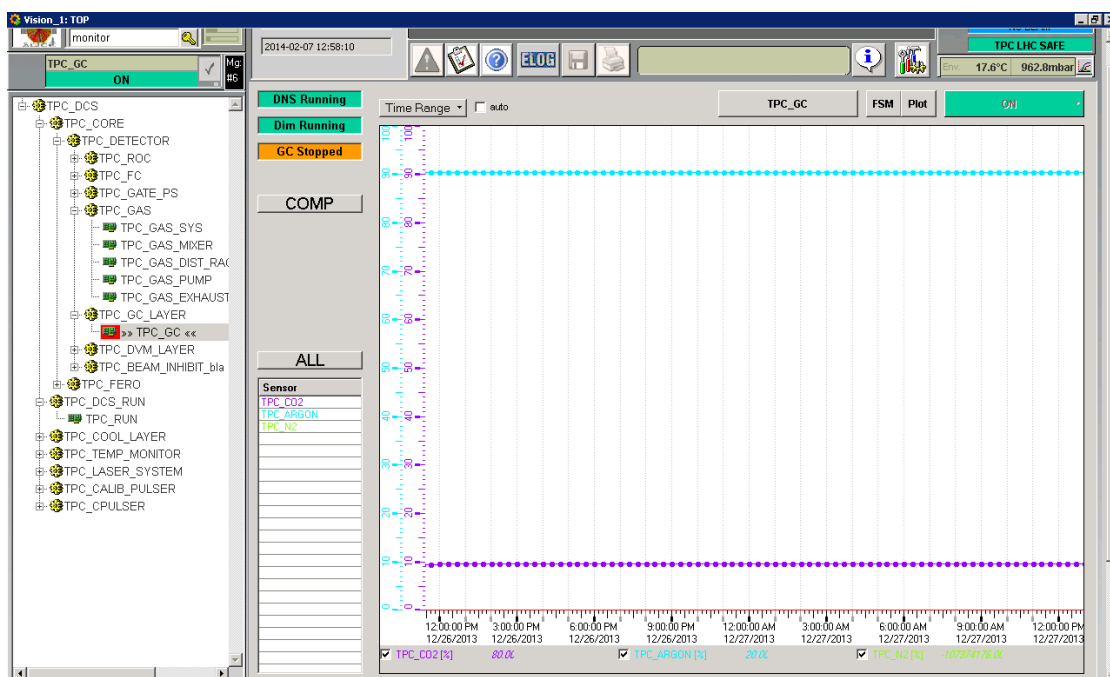


Figure 3.2.: The WinCC panel of the gas chromatograph in the TPC detector control system. The central feature is a trending plot that shows the gas composition as a function of time. Blue points show the fraction of argon, purple points the fraction of CO₂ in the gas mixture.

3.2. WinCC panel

A panel for display of the gas composition data sent to WinCC-OA has been created and set up in the TPC and TRD detector control system (fig. 3.2). The central feature is a trending plot, that shows the gas composition as a function of time. Data points are stored in a central database. The status of the DIM DNS server, WinCC-OA DIM client and the DIM server of the gas chromatograph are indicated in the top left of the panel. Alarms can be set to automatically generate notifications when the gas composition values are off limits.

A similar panel as shown in fig. 3.2 for the TPC DCS is available in the TRD WinCC control system.

3.3. Setup Stability

A natural requirement for the setup is to run continuously over long periods of time. The installation of the software for the gas chromatograph that was intended to be final was made on a virtual Windows 7 machine running on one of the existing DCS servers. The software can not be installed directly on one of the DCS Windows servers, as Agilent OpenLAB CDS ChemStation requires Windows 7, Vista SP1 or XP SP3 as operating system. Using a virtual machine with the appropriate

operating system provides several benefits, e.g. stable server hardware, straight forward connection with the network and straight forward possibility for remote access, easy administration etc.

In a first long-term testing run of the gas chromatograph and DIM setup, it turned out that after a few days of continuous operation, a software error caused the system to stop measuring and accept further commands. The error was traced back to a characteristic series of events in Agilent ChemStation that were logged by the event viewer of the operating system, of which the final entry reads “Connecting with GC in pre-run state; forcing an idle state”. The GC would stay idle until restarting ChemStation.

Stability was not a problem when the software was operated from a desktop computer, to which all of the GC periphery could be connected directly and it was decided to again operate the Chromatograph from within this machine. This computer is located in SG2, is presently connected to the network and can be reached remotely via Virtual Network Computing (VNC) software to control the GC. This setup did not show any irregularities during a month of continuous operation. The error that was seen before can thus be attributed to the complication that is introduced by a virtual machine (e.g. no physical connection with the periphery of the chromatograph and the network, etc.).

4. Calibration

The TCD signal peak area is proportional to the amount of gas. However the constant of proportionality is a different one for each substance. To obtain precise results, calibration is necessary. In principle, calibration is achieved by measuring a reference gas of known composition.

For this thesis, calibration was implemented in two distinct ways. However, both methods rely on the assumption, that the TCD signal peak area as function the amount of substance is a line through the origin. A third option that is free of this assumption is briefly discussed in the prospects (section 6).

4.1. Absolute calibration

The first method of calibration that can be done with the current setup yields the absolute amount of each gas component that is analysed in each run. A measurement of a reference gas with known gas composition is done and for each of the i peaks, a response factor r_i can be calculated:

$$r_i = \frac{\text{peak area}_i}{\text{amount of substance } i} \quad (4.1)$$

Hence, the fraction f of each component in the gas mixture is

$$f = \frac{n}{\sum_i n_i} = \frac{\text{peak area}}{r_i \cdot \sum_i \frac{\text{peak area}_i}{r_i}} \quad (4.2)$$

The difficulty is to obtain the proper amount of substance. Gas chromatography is often done on liquids that can be evaporated without dissociation, for which the amount of substance is obtained via the sample mass, that is easily measured with a scale. For gaseous compounds, assuming ideal gas behavior, the amount n_i of substance i is given as

$$n_i = \frac{pV_i}{RT} \quad (4.3)$$

with pressure p and temperature T measured at sampling time, the gas constant R and the volume of the sampling loop, multiplied with the gas fraction of compound in the reference mixture: $V_i = V_{\text{sampling loop}} \cdot f_i$.

The downsides of this method are:

- The pressure sensor that is nearest to the sampling loop is analog and requires manual readout.
- The pressure measurement is not in situ. Between sensor and sampling loop is about 1m of tubing resulting in a pressure drop that can only be estimated.
- It is assumed that the graph of the peak area as a function of the amount of substance is a line through the origin.
- Ideal gas behavior is assumed, which is an approximation.

The response factors obtained with this method are

$$r_{\text{CO}_2} = 1.005 \times 10^{12} \frac{25\mu\text{V}}{\text{mol}} \quad (4.4)$$

$$r_{\text{Xe}} = 1.014 \times 10^{12} \frac{25\mu\text{V}}{\text{mol}} . \quad (4.5)$$

4.2. Automated relative calibration

The second method of calibration does not use absolute amounts of substance, but calibrates relative peak areas to fit the expected composition of the reference gas. The approach is similar to the method described above.

We denote the peak area of two peaks with A_1 and A_2 .

The relative area of peak i is

$$a'_i = \frac{A_i}{A_1 + A_2} \quad (4.6)$$

We can introduce a calibration factor α for one of the two peaks (or in general: $N - 1$ constants for N peaks), such that its measured relative peak area is similar to the fraction f of the compound in the reference gas:

$$\alpha \cdot A_2 = f \quad (4.7)$$

The two calibrated relative peak areas are then:

$$a_1 = \frac{A_1}{A_1 + \alpha A_2}$$

$$a_2 = \frac{\alpha A_2}{A_1 + \alpha A_2}$$

The advantage of this method is that with the powerful combination of WinCC, a freely programmable DIM server and the information in the measurement output files, a full automation of the above calibration steps can be achieved easily, such that a calibration is repeated after a certain time and the resulting calibration factor is updated in WinCC.

The downsides are:

- It is assumed that the graph of the peak area as function the amount of substance is a line through the origin.
- This method is accurate only at the reference gas composition and as more contamination accumulates in the detector gas, calibration gradually grows inexact.
- If the TCD response is not a line through the origin, this method is accurate only when the same amount of substance is injected in a measurement and the calibration process.

5. Maintenance

Whereas the ordinary measurement operation is fully automated, some maintenance is required in extraordinary situations.

The exit of the TCD is a simple vent, releasing the sample and carrier gas into the surroundings after an analysis. Carrier gas is continuously flowing through the columns and make-up gas is continuously mixed to the column flow before entering the TCD. Because of this continuous venting of helium, a replacement for the helium bottle that is used as supply of carrier and make-up gas must be replaced about once every three months.

Over time, the columns collect water which changes retention times for all substances passing a column. Additionally, the molecular sieve in column 2 can reach a saturation point when it can no longer absorb additional CO₂.

The columns can be restored to their usual behavior by heating the columns (an oven temperature of 150 °C is used currently). There must be active carrier gas flow and valve 2 must be off (in order to enable flow through column 2) during this process. A method has been created that can be used to recondition the columns in this way.

The ALICE chromatograph is supposed to run continuously until the end of the LHC physics program. Major changes to the gas composition (such as the recent change from a Ne-CO₂-N₂ to a Ar-CO₂ mixture for the TPC) require an update to the peak identification procedure of the DIM server and may require an update of the chromatographic method.

6. Summary and prospects

An automated measurement of the gas composition of the ALICE TPC and TRD with the use of a gas chromatography system has been put into operation and integrated into the ALICE detector control system. For this purpose, chromatography methods that achieve proper separation of the components have been created. Separation and detection of xenon, argon, neon, nitrogen, oxygen and CO₂ has been performed successfully and calibration has been carried out.

A DIM server providing the link between the chromatography system and the TRD and TPC WinCC-OA detector control system has been developed. WinCC-OA panels for displaying the analysis results have been composed and integrated into the control system of the ALICE TPC and TRD.

Long-term stability has been established.

Recently, column 1 has been replaced by a different model, since with the original column, separation of xenon and CO₂ was not possible without cooling the columns. The new column is capable of separating the TRD gas.

Calibration relies on the assumption that the thermal conductivity detector signal as a function of time is a line through the origin. A two point calibration for all peaks could be implemented, if a further gas mixture featuring different concentrations of all gases in question, e.g. 79%CO₂, 10%Xe, 10%Ar ,1% N₂ would be available. In principle, this is already possible for CO₂, as the TRD and TPC gas have different CO₂ concentrations.

Part II.

**Measurement of electrons from
semi-leptonic heavy-flavour hadron
decays in p-Pb collisions at
 $\sqrt{s_{\text{NN}}} = 5.02 \text{ TeV}$ with the ALICE
TRD**

7. Motivation

The study of the properties of the quark-gluon plasma (QGP) is carried out as a comparison between pp and Pb-Pb collisions. Since there already is a conceptual difference between a single free proton and strongly bound protons in a nucleus, there needs to be a third reference to identify effects that specifically arise due to non-QGP nuclear effects. Proton-lead collisions provide this reference. The observable that is used to provide a comparison between pp collisions and collisions of two nuclei AA is the so called nuclear modification factor R_{AA} defined as:

$$R_{AA} = \frac{dN^{AA}/dp_T}{\langle T_{AA} \rangle d\sigma^{pp}/dp_T}, \quad (7.1)$$

with the differential particle yield in nucleus-nucleus collisions dN^{AA}/dp_T , the differential cross section in pp collisions $d\sigma^{pp}/dp_T$ and the nuclear overlap function $\langle T_{AA} \rangle$, which is the expectation value for the number of binary pp collisions when two nuclei AA collide, divided by the total inelastic cross section of nucleon-nucleon interactions. Thus the product of the nuclear overlap function $\langle T_{AA} \rangle$ and the pp cross section is an estimation for the particle yield in nucleus-nucleus collisions, that holds true as long as there are no additional phenomena taking place besides the increased number of binary nucleon-nucleon collisions. Consequently a R_{AA} that differs from unity suggests suppressing or enhancing effects that can give hints towards the existence and the properties of the QGP.

Studying the quark-gluon plasma is in many ways similar to the Rutherford experiment, where details of scattering processes lead to conclusions on the structure of matter. In the case of Geiger, Marsden and Rutherford, however, the target (a gold foil) was constantly at a known position whereas the quark-gluon plasma only has a short lifetime of about $10 \text{ fm}/c \approx 3.3 \times 10^{-23} \text{ s}$ [17]. Additionally, collisions are distributed around the nominal center of ALICE, such that the location in beam direction of the primary vertex is within $\pm 10 \text{ cm}$ of the nominal center for 90% of the events. Trying to hit the overlap region of two colliding nuclei with an external probe just after the collision is not a viable option.

Nature fortunately provides us with auto-generated internal probes: Heavy quarks. Only hard scattering processes that happen in the initial phase of a collision are energetic enough that heavy quarks, such as bottom and charm, are produced. The number of heavy quarks is conserved throughout the collision, since due to their high mass there is no subsequent production in thermal processes and the cross section of quark-antiquark annihilation is small enough to be neglected [18]. As heavy quarks are created initially and their lifetime is longer than that of the

QGP, they experience the entire evolution of the system. Hence, heavy quarks are a unique probe to study the quark-gluon plasma. Large branching ratios and high signal-to-background ratios at high transverse momenta are some of the advantages of the electron channel.

Measurements of electrons from heavy-flavour hadron decays in p-Pb collisions have already been made with the ALICE TPC and TOF [19]. As the ALICE TRD is specifically designed to provide electron identification at momenta larger than 1 GeV/ c , where the electron-pion separation with the TPC energy loss measurement becomes increasingly challenging towards higher momenta, the TRD is predestined for this kind of analysis. The powerful hadron discrimination of the TRD is high enough to make a subtraction of hadron contamination to up to a transverse momentum of 6 GeV/ c unnecessary, resulting e.g. in lower systematic uncertainties and an improved separation of electrons and hadrons. Thus, the TRD allows to substantially extend the viable p_T range towards high transverse momenta. In this analysis, measurements from a transverse momentum of 2 GeV/ c up to 12 GeV/ c are presented.

The goal of this analysis is to measure the spectrum of electrons from semi-leptonic heavy-flavour hadron decays in p-Pb collisions at $\sqrt{s_{NN}} = 5.02$ TeV with the ALICE Transition Radiation Detector and finally to give a physics result in the form of the nuclear modification factor R_{pPb} .

8. Introduction

An analysis similar to the measurement of electrons from semi-leptonic heavy-flavour hadron decays in p-Pb collisions at $\sqrt{s_{\text{NN}}} = 5.02 \text{ TeV}$ using the ALICE TPC and TOF [19] is carried out here with the ALICE TRD instead of the time of flight measurement. The TRD extends the viable measurement range towards higher transverse momenta. This analysis closely follows the TPC-TOF example, concerning the dataset and the majority of the selection cuts.

In this chapter, an overview of the analysis steps, the dataset, the event selection cuts and track selection cuts are given.

8.1. Outline of the analysis

The analysis consists of the following steps:

1. Event selection (reject e.g. beam-gas collisions).
2. Select high quality tracks using various cuts on TPC and ITS.
3. Identify electron candidates with TRD and TPC PID cuts.
4. Correct the measurement for efficiency and acceptance.
5. Subtract the cocktail of background electrons.

This procedure will result in a spectrum of semi-leptonic electrons from heavy-flavour hadron decays from which a physics comparison with pp collisions in the form of R_{pPb} can be calculated.

The details of these steps are described in the following chapters.

8.2. Dataset and Monte Carlo simulation

The data used in this analysis is the minimum bias p-Pb Event Summary Data (ESD) of the periods LHC13b and LHC13c (ALICE internal naming convention, used to identify the various LHC data taking periods). These add up to 1.21×10^8 triggered events before event selection. A list of all ESD run numbers and their relative contribution to the total event count can be found in appendix B, tab. B.1. Minimum bias Monte Carlo simulations LHC13b2_efix1, 3 and 4 (ALICE internal naming convention) are used that were created with the DPMJET generator [20].

The minimum bias trigger that is used requires a coincidence of signals in both V0 detectors (“V0AND”). Furthermore, a Monte Carlo simulation featuring an increased number of B and D mesons is used, so that there are more semi-leptonic decays of beauty and charm quarks per event. This signal-enhanced simulation, LHC13d3, was generated with HIJING [21]. The Monte Carlo simulations are anchored to the data runs, so that the actual running condition of each run is reproduced in the simulation.

8.3. Event Selection

The event selection criteria are the same as in [19]: Good events have to have at least one Silicon Pixel Detector (SPD) vertex and a primary vertex with at least one contributor. Additionally, the difference in z between both vertices has to be smaller than 0.5 cm. The resolution in z (beam axis) of the SPD vertex is required to be less than 0.25 cm. The position of the primary vertex along the beam axis must be located within 10 cm of the nominal center of ALICE.

When using the TRD for tracking, its wake-up efficiency of 99.5% needs to be respected. The default state of the TRD is in stand-by, in which all digital clocks are switched off, minimizing electronic noise [5] (and power consumption). A pre-trigger is used as wake-up signal before a read out is initiated. This wake-up happens with a certain efficiency. The total number of recorded events is reduced by 0.5% when TRD tracking data is required.

8.4. Track selection

Cuts to individual tracks are applied in order to select only those tracks that suit the analysis. Only tracks with pseudorapidity of $|\eta| < 0.49$ are accepted, as an η dependency of the TPC signal for $0.6 < |\eta| < 0.9$ causes significant variation in its particle identification properties. The decision to reduce the range even further was made in order to not include the stack border of the TRD. A rough value of the η position of the stack border can be inferred from fig. 10.1. The actual values are obtained from alignment data.

A complete list of track selection cuts for electron candidates is given in table 8.1. The requirement for tracks with two hits in the innermost ITS layers, the silicon pixel detector (SPD), is to eliminate background from photon conversion in detector material beyond the SPD. The high number of 110 required TPC clusters for a good track takes advantage of the higher energy loss of high momentum electrons passing through matter compared to other particles. Consequently, electrons produce a higher signal in the TPC and requiring a high number of clusters intrinsically prefers electron over hadron tracks.

Observable	Cut value
TPC and ITS refit	required
$\chi^2/\#\text{TPC cluster}$	< 4
Kink daughters	rejected
Number of ITS clusters	≥ 4
Requirement SPD pixels	both
Number of TPC clusters	≥ 110
Number of TPC dE/dx clusters (PID clusters)	≥ 80
Ratio found/findable TPC clusters	> 0.6
DCA to the primary vertex in radial direction	$< 1 \text{ cm}$
DCA to the primary vertex in z-direction	$< 2 \text{ cm}$

Table 8.1.: Track selection cuts [19].

9. Particle identification

In this analysis we use the ALICE TPC and TRD for particle identification (PID), utilizing the electron identification capabilities of the ALICE TRD. In the TPC-TOF analysis [19], the electron spectrum from heavy-flavour hadron decays was studied for transverse momenta from $0.5 \text{ GeV}/c$ to $6 \text{ GeV}/c$. The idea is to complement the TPC-TOF measurement at higher momenta using the TRD.

To produce transition radiation, a particle must exceed a critical $\beta\gamma$ value (compare equation 1.4 on page 4). Thus, low momentum electrons can not be studied with the TRD. Electron identification with the TRD becomes viable for momenta larger than $1 \text{ GeV}/c$ [5]. Naturally, particle identification with the time of flight detector is limited to momenta for which the particle species that are to be distinguished have significantly different velocities. Due to the efficiency and acceptance of the time of flight detector, 14% of electron tracks (tracks used for this crosscheck are electron tracks from V0 decays with $|\eta| < 0.5$ and a transverse momentum between $2 \text{ GeV}/c$ and $5 \text{ GeV}/c$) are lost when additional to TRD and TPC tracking, TOF PID and tracking is requested. We therefore omit the usage of the TOF completely, as opposed to use the cascade of TPC-TOF-TRD. As a consequence, the low momentum regime, where the electron line is intersected by hadron lines in the TPC dE/dx versus momentum distribution (fig. 9.1a), can not be analysed.

In contrast to this analysis, the TPC-TOF analysis focuses on the low momentum regime and uses the time of flight detector to separate the crossing lines of kaons (at $\approx 0.5 \text{ GeV}/c$), protons (at $\approx 1 \text{ GeV}/c$) and deuterons (at $\approx 2 \text{ GeV}/c$) from the electron line in the TPC dE/dx signal (fig. 9.1).

It is evident, that the PID quality of the TRD improves when the pulse height spectrum (fig. 1.4 on page 5) can be measured multiple times for the same track, or in other words, PID quality improves, when a track is measured with a high number of TRD tracklets: The parts of a track that are measured by the individual chambers of the TRD. Therefore only tracks that were measured with exactly five or with exactly six tracklets are used in this analysis.

A TRD PID cut with an electron efficiency of 53.3% is applied, resulting in a hadron rejection factor of the order of 510, thus $1 - \frac{1}{510} \approx 99.8\%$ of hadrons are removed at the cost of 47% of electrons. Exact evaluation of the hadron rejection factor requires to study the contribution of different hadrons separately, which was not done here. The estimation of the hadron rejection factor of 510 given here, is the mean reduction of all hadrons in fig. 9.2 in the TPC $\frac{dE/dx - \langle dE/dx \rangle_e}{\sigma_{dE/dx}}$ range between -8 and -4 . The above TRD PID cut includes a cut on missing slices: A tracklet is discarded for PID, when one or more time bins of the readout of a TRD

chamber contain no signal (compare section 1.2 on page 4).

The effect of the TRD PID cut is demonstrated by fig. 9.1, where the TPC PID dE/dx signal with and without the use of TRD PID is given for comparison. With applied TRD PID, the TPC energy loss signal (9.1b) shows an extreme reduction of pions and high momentum hadrons. Additionally, the region separating the electron band from the pion and high momentum hadron regime increases significantly compared to the measurement without TRD PID.

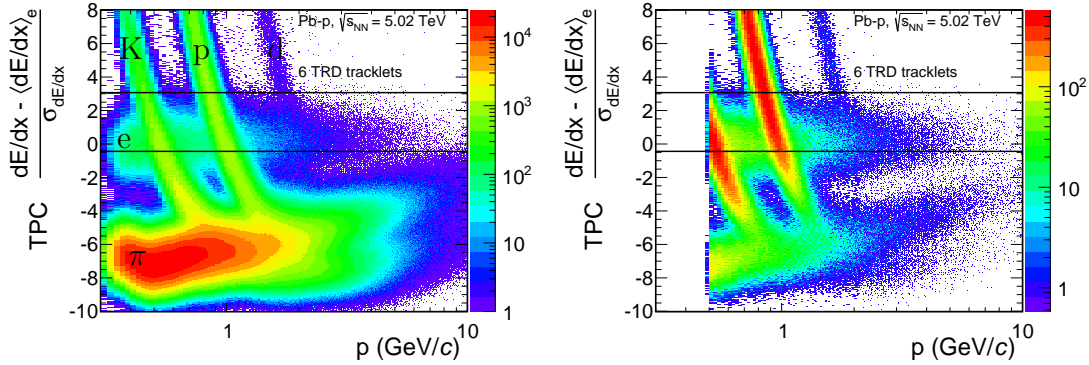
A further assessment of the TRD hadron rejection is obtained by projecting the content of the histograms of fig. 9.1a and 9.1b to the vertical axis (fig. 9.2). The projection was done only for tracks with momenta larger than $2.6 \text{ GeV}/c$, in order to safely exclude the momentum regime where the hadron crossing lines intersect with the electron line. For the pure TPC measurement, the electron signal is heavily contaminated by the tail of the huge hadron peak. With additional TRD PID, the hadron peak is massively reduced and the peaks are separated more clearly.

After the TRD PID cut, a cut on the TPC dE/dx signal is applied, accepting only tracks with $-0.5\sigma_{\text{TPC-}dE/dx} < dE/dx < 3\sigma_{\text{TPC-}dE/dx}$ around the electron hypothesis. On the low end of the electron signal, where the electron and pion signals mix, the rather strong cut at -0.5σ is applied in order to further minimize hadron contamination. The upper end of the electron signal is cut loosely at 3σ , as no contamination is expected for the momentum regime beyond the crossing of the deuteron line and the electron line.

The hadron contamination as a function of particle momentum p for tracks with a momentum higher than $4 \text{ GeV}/c$ is quantified in fig. 9.3. These curves are obtained in two steps. In several momentum slices of the TPC $n\sigma$ distribution (fig. 9.2), a fit to the hadron and electron contribution is made (the details of this procedure can be found in [22]). For the used data sample, fits with reasonable statistics are obtained up to a maximum momentum of $10 \text{ GeV}/c$. The overlap region describes the hadron contamination in the respective momentum bin. The set of all hadron contamination values obtained in this way is fitted with an error function in order to obtain a curve as given in fig. 9.3 that further serves as an extrapolation of the hadron contamination from $10 \text{ GeV}/c$ up to $12 \text{ GeV}/c$.

Contamination from low momentum hadrons (crossing lines) is not depicted in this graph. The minimum transverse momentum that is analysed in this thesis will be chosen such that low momentum hadron contamination is cut away (compare fig 10.5 on page 61). The subtraction of hadron contamination that is done in the course of this analysis is based on the functions shown in fig. 9.3, by assigning a weight to each track that corresponds to the hadron contamination fraction at the respective track momentum. Hadron contamination is removed bin-wise, by subtracting the sum of the weights for all tracks in the regarding bin. The hadron contamination for momenta larger than $10 \text{ GeV}/c$ is extrapolated from the data at lower p values.

The comparison between the hadron contamination using only TPC cuts and the performance with applied TRD PID (fig. 9.3) again demonstrates the merit that is contributed to the analysis by the TRD particle identification. With TRD



(a) Without TRD particle identification. (b) With TRD particle identification applied.

Figure 9.1.: Energy loss of charged particles as measured by the TPC as a function of momentum. The expectation value of the electron hypothesis is shifted to zero and is normalised to a standard deviation of the energy loss signal. For these plots, only tracks with six TRD tracklets have been used. Results with (b) and without (a) TRD PID reveal the TRD hadron rejection capabilities. TRD PID is not applied on tracks with momenta lower than $0.5 \text{ GeV}/c$ and corresponding tracks are not shown in (b). The black horizontal lines show the PID cut of $-0.5\sigma_{\text{TPC-dE/dx}} < dE/dx < 3\sigma_{\text{TPC-dE/dx}}$ applied to the TPC signal.

PID, there is practically no hadron contamination up to a momentum of $6 \text{ GeV}/c$, whereas hadron contamination is relevant already at $4 \text{ GeV}/c$, when solely applying the TPC cut of $dE/dx > -0.5\sigma_{\text{TPC-dE/dx}}$, that is used in this analysis. Naturally the hadron rejection of the TRD improves with increasing number of tracklets and thus more independent measurements of the pulse height spectrum (fig. 1.4 on page 5), which are used for discerning electrons and pions. Therefore, hadron contamination is significantly lower for the six tracklet case than for the five tracklet case.

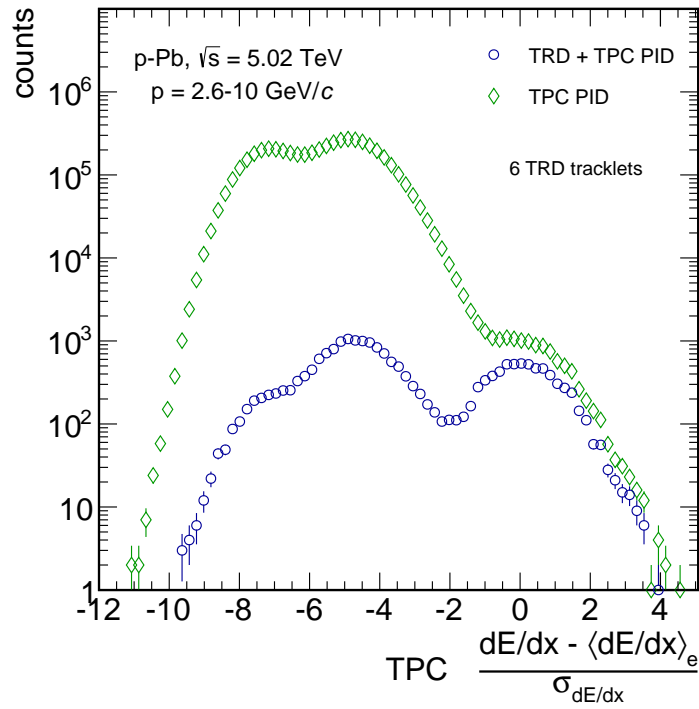


Figure 9.2.: The number of particle tracks in the momentum range from 2.6 GeV/ c to 10 GeV/ c as a function of TPC dE/dx subtracted by the electron hypothesis in units of the standard deviation shows the hadron rejection capability of the TRD: Green diamonds show the number of particles using TPC PID only. In blue circles, the same data is shown with applied TRD PID cut for an electron efficiency of 53.3%, that is used in this analysis. The number of electrons (peak centered around zero) is reduced to 53.3%, whereas the number of pions is reduced dramatically to only 0.02%, resulting in a much lower pion contamination of the electron candidate sample.

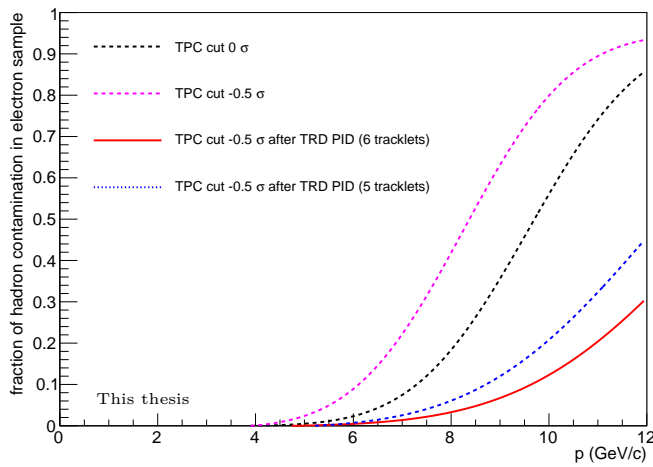


Figure 9.3.: Hadron contamination for particle momenta larger $4 \text{ GeV}/c$ as a function of particle momentum p for the PID cuts that are used for the TPC and TRD [23]. With applied TRD PID, there is nearly zero hadron contamination up to $6 \text{ GeV}/c$ instead of about 10% using the TPC only. At $10 \text{ GeV}/c$, the TPC-only PID strategy yields an unusable fraction of about 80% hadrons in the electron candidate sample that is reduced to below 15% with TRD PID and six TRD tracklets. The hadron contamination for momenta larger than $10 \text{ GeV}/c$ is extrapolated from the data at lower p values.

10. Efficiency and efficiency correction

Not all electrons that are produced in a collision

- propagate where detecting material is present (the detector has finite geometrical acceptance),
- can be reconstructed (finite reconstruction efficiency),
- are identified correctly as electrons (finite electron identification efficiency) and
- pass event and track selection and particle identification cuts.

In what follows, we denote the group of these effects with the term efficiency. As a consequence of the limited efficiency, more electrons are produced in the collisions than can be measured in the detector and this effect must be corrected for. The chosen operating point of the TRD PID cut is an electron cut efficiency of 53.3% (compare chapter 9). The TPC electron identification efficiency is estimated to be 69% for the applied PID cut of $-0.5\sigma_{\text{TPC-dE/dx}} < \text{dE/dx} < 3\sigma_{\text{TPC-dE/dx}}$, assuming a gaussian shape of the TPC electron signal [19].

The efficiency correction is done using a Monte Carlo simulation of the detector that is exposed to simulated events. In the simulation, full information of each track is available. Comparing the true number of particles with the measured number of events yields the efficiency of the detector with the applied cuts.

It is evident that an accurate representation of the real world detector in Monte Carlo is crucial for this step. Therefore this aspect is reviewed in detail in the following section.

10.1. Refining the implementation of the TRD in the Monte Carlo simulation

The implementation of the active area of the TRD in the Monte Carlo simulation was assessed, using histograms that show the number of detected charged particles on an η - ϕ plane of a single layer of the TRD (fig. 10.1). For all layers of the TRD, histograms analogue to fig. 10.1 were created for data and Monte Carlo, using only tracks of positive charge with a reconstructed transverse momentum larger than

2 GeV/ c . The applied p_T cut results in a sample that is not too strongly affected by the magnetic field. By restricting the sign of the charge, all tracks are bent in the same direction by the magnetic field. Otherwise, double contours prevent a clear picture.

The used η and ϕ information is based on the combined track reconstruction and reflects the respective track parameters at the vertex. Due to the magnetic field, these η and ϕ values do not reflect the track parameters at the respective TRD chamber. Yet, the precision of this information is sufficient in order to attribute differences between data and Monte Carlo to individual (half) chambers of the TRD (compare fig. 10.2) which is the task at hand.

In the two white areas centered at around $\phi \approx 1.7$ and $\phi \approx 4.7$ that cover the whole η range, no super modules have been installed during the 2013 LHC runs. The middle chamber of the supermodule centered at $\phi \approx 5.3$ is left out on purpose to reduce the material budget for the photon spectrometer (blue structure at the very bottom of fig. 1.5) that is located beyond the TRD. The other white chambers are either mapped out due to known problems during that data taking run (e.g. problems with the front end electronics or the chamber high voltage) or mapped out due to misrepresentation in the Monte Carlo simulation, as is described below. Normalizing these histograms to their total event count and plotting their difference, reveals chambers that are not represented well in Monte Carlo (fig. 10.2). The ratio of both histograms is not well suited as indicator, as for ratios, an empty bin in the numerator as well as in the denominator results in an empty bin in the resulting histogram. Thus no information is obtained, whether e.g. a complete chamber is missing in one of the histograms that are divided. This check was done on a per-run basis.

The status of the chambers found in this way (tab. 10.1) has been updated in the offline conditions database (OCDB) and they were not used in the remaining analysis. All data from the corresponding chambers is ignored for TRD PID, the deposited charge in the relevant chambers is set to zero and the number of tracklets is recalculated. As the TRD does not contribute tracking information to the combined track reconstruction, a recalculation of global tracking information is not required.

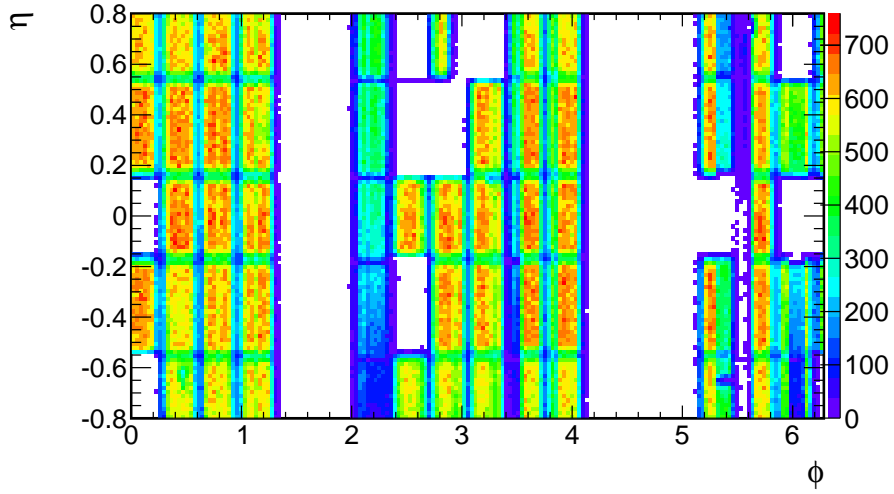


Figure 10.1.: Number of entries in layer 3 of the TRD as a function of η and ϕ in data run 195531 (ALICE internal convention for run identification). Only tracks of positive charge with a reconstructed transverse momentum larger than $2 \text{ GeV}/c$ are shown. In the two white areas centered at $\phi \approx 1.7$ and $\phi \approx 4.7$ no super modules have been installed during the 2013 LHC runs (compare fig. 1.5).

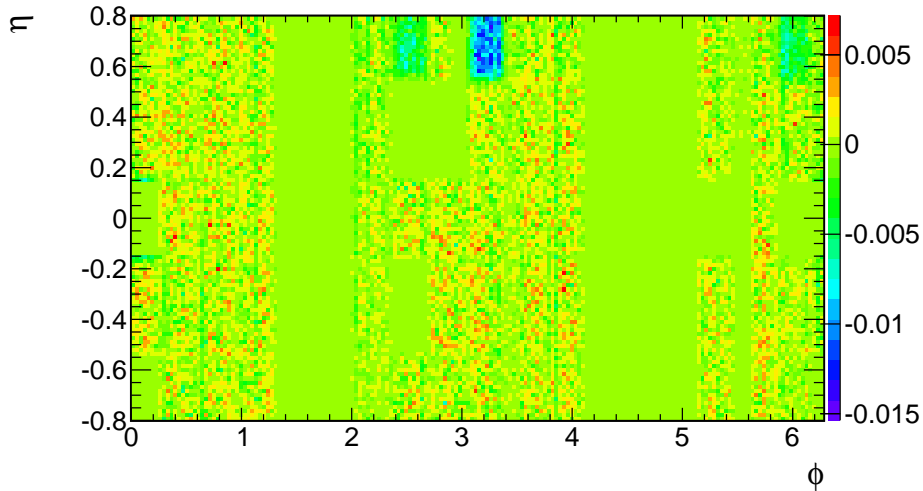


Figure 10.2.: Difference of η - ϕ maps obtained from data and from the Monte Carlo simulation for the same tracks that were used for fig. 10.1. The three chambers that show abnormal deviation from zero (centered at $\eta = 0.7$, and $\phi = 2.5, 3.2$ and 6) were removed for the analysis and are also mapped out in fig. 10.1.

run	super module	stack	layer	chamber	reason
195483	1	2	4	46	front end electronics (FEE)
195633	9	2	5	287	High Voltage (HV)
195635	10	4	1	325	HV
195673	15	0	5	455	FEE
for all runs	11	0	4	334	HV
	8	0	4	244	
	9	0	3	273	HV
	17	0	3	513	HV
	7	3	2	230	HV
	7	0	3	213	HV
	0	2	3	15	

Table 10.1.: TRD chambers that are disabled in the analysis due to discrepancies that are seen between data and the Monte Carlo simulation. The contribution of the runs to the total event count can be found in the appendix B, tab. B.1.

10.2. Validation for using Monte Carlo efficiency correction

A precise representation of the TRD data of the LHC13b and LHC13c periods in the Monte Carlo simulation is an important premise to use the efficiency correction based on Monte Carlo. To further check if the active area of the TRD is implemented well in the Monte Carlo simulation, a method to quantify the TRD tracking efficiency that is independent from the Monte Carlo based method is used and results are compared between data and Monte Carlo. For this independent method, electrons from V0 decays are used to obtain the tracking efficiency and acceptance as a function of transverse momentum. A V0 decay is a decay of a photon via photon conversion: A neutral secondary vertex decaying into an opposite sign dielectron pair. The decay produces V-shaped tracks and the net charge is 0, hence the name “V0”. By use of geometrical cuts and calculation of the invariant mass of the photon, electrons from V0 decays can be identified. In this way, a clean electron data sample is obtained without the use of TRD PID.

Comparing the number of remaining particle tracks before and after demanding the TRD tracking cut, hits in either exactly five or exactly six layers of the TRD, yields the TRD tracking efficiency and acceptance for five or six tracklets respectively. As this step is a division of two histograms where one histogram contains a subset of entries from the other, uncertainty values have been propagated using binomial statistics.

The curve of the tracking efficiency obtained in that way (fig. 10.3 for five tracklets

and fig. 10.4 for six tracklets) is expected to reach zero towards low p_T , since low momentum tracks are not able to propagate far enough to reach the TRD. For high p_T values it is expected to be constant as all electrons have equal probability to create a signal in the TRD. The transition between both transverse momentum regimes, where gradually more tracks are able to reach the TRD, is described well with an exponential term. A fit of

$$\epsilon(p_T) = a \left(1 - e^{-b(p_T - c)}\right) \quad (10.1)$$

with free parameters a , b and c is a good description of the data. The fit results for the five and six tracklet measurements are

$$a = 0.1214 \pm 0.0006, b = 13.37 \pm 0.46, c = 0.313 \pm 0.001 \text{ (five tracklets)}$$

$$a = 0.2752 \pm 0.0062, b = 12.97 \pm 0.11, c = -0.047 \pm 0.035 \text{ (six tracklets)}.$$

At low transverse momentum, this measurement of the efficiency shows considerable deviation between the minimum bias Monte Carlo simulation and data. This could be caused by an improper implementation of the material budget of the detector in the Monte Carlo simulation, from which low p_T tracks are affected more strongly. A comparison between data and Monte Carlo simulation in the transverse momentum range of 2.3 GeV/ c to 4.5 GeV/ c , which is the p_T range that is used below for comparison with the TPC-TOF results, is compatible with unity within the uncertainties for both the five and the six tracklet case. A constant fit to this ratio from 2.3 GeV/ c to 4.5 GeV/ c yields 0.946 ± 0.068 (1.000 ± 0.045) for five (six) tracklets.

A track results in a five tracklet TRD measurement, that is a track that has exactly five TRD tracklets, either if the track is propagating through a stack with one chamber missing, or if the charge deposition in one chamber is not sufficient to produce a tracklet, or if the track is bent in a way that its trajectory does not traverse the chamber in the highest or lowest layer. These cases are exceptions - the six tracklet case has a higher geometrical acceptance, as there are more stacks that have all chambers working than there are stacks where a chamber in one or more layer is out of order. Therefore the plateau value of the efficiency and acceptance curve for the six tracklet case has with nearly 30% about double the value of the tracking efficiency and acceptance for the five tracklet case. The regime where a constant plateau is reached in the efficiency and acceptance curve, is beginning at higher transverse momentum values for the six tracklet case than it is for five tracklet measurements, as straighter tracks are required to intersect with all six chambers of a stack.

The fit range used to compare the efficiencies is the same that is used later to compare the resulting particle spectrum with the TPC-TOF analysis. Since the time of flight detector is not used in the TRD analysis, the kaons, protons and deuterons that are present in the low p_T range of the spectrum (fig. 10.5) are indistinguishable from electrons and contaminate the spectrum with peak structures. The fit must start at a higher p_T value than that of the deuteron contamination

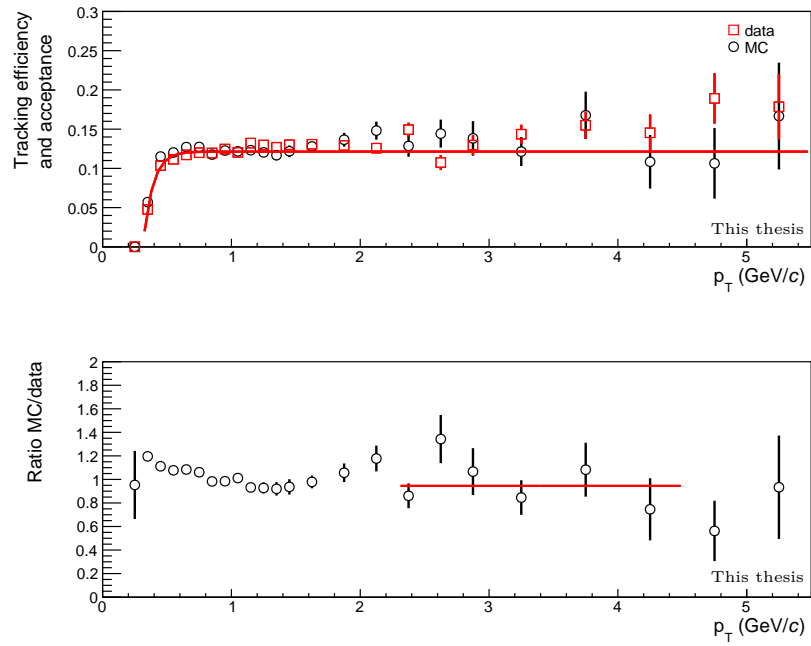


Figure 10.3.: Top: Comparison of TRD tracking efficiency using V0 electron data and the minimum bias Monte Carlo simulation with exactly five TRD tracklets.
 Bottom: The ratio of the two distributions. A constant fit from 2.3 to 4.5 GeV/c yields 0.946 ± 0.068 .

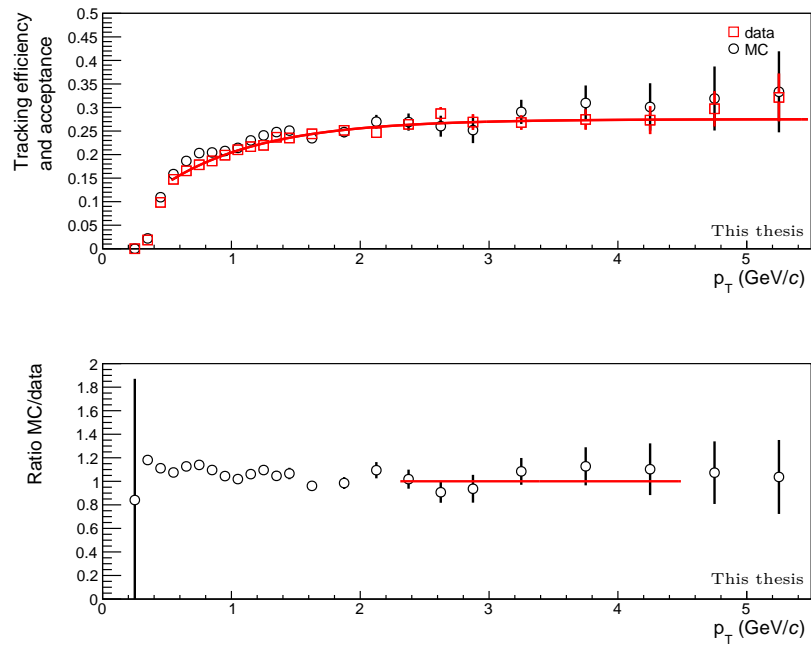


Figure 10.4.: Six tracklet case of fig. 10.3. A constant fit from 2.3 to 4.5 GeV/c yields 1.000 ± 0.045 .

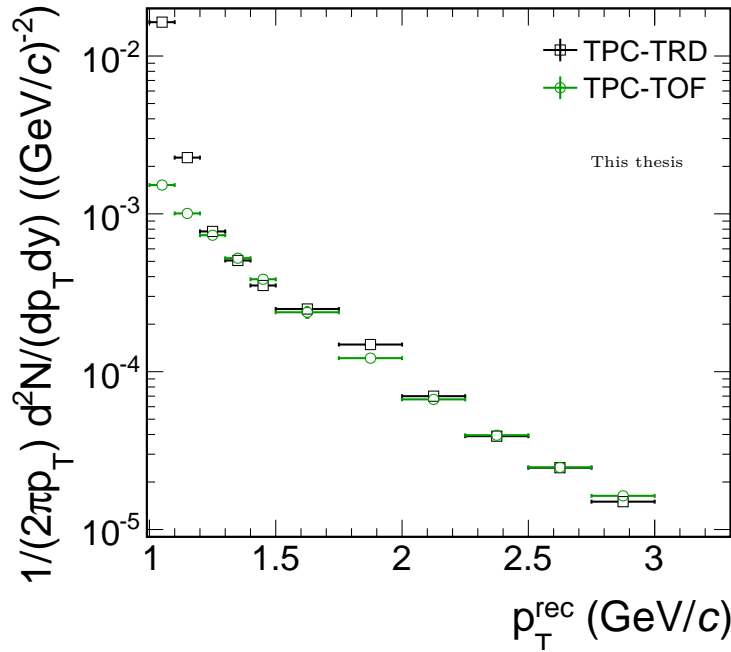


Figure 10.5.: Zoom into the low end of the inclusive electron spectrum, measured with TPC-TRD, in comparison with the TOF-TPC result. Since the time of flight detector is not used in the TRD analysis, the kaons, protons (two leftmost points) and deuterons (slight excess in the range $1.5 \text{ GeV}/c$ to $2.2 \text{ GeV}/c$) that are present in the low p_T range of the spectrum can not be distinguished from electrons and contaminate the spectrum with peak structures. The fit that is used later for comparison with the TPC-TOF analysis starts at $2.3 \text{ GeV}/c$, because the high p_T end of the deuteron feature is absent from this point onwards. A crosscheck with fig. 9.1 holds. The spectrum of the TPC-TOF analysis is plotted in order to identify the transition from the deuteron feature to the power law behaviour of the inclusive electron spectrum.

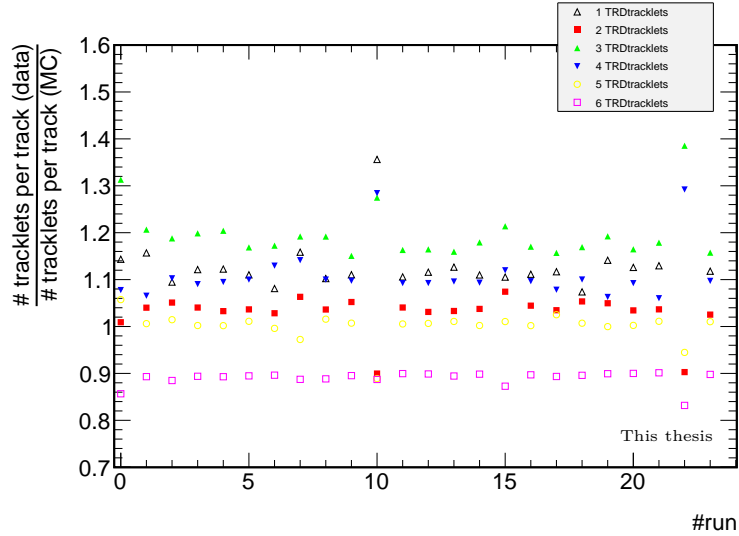


Figure 10.6.: Ratio of the number of TRD tracklets per track for individual runs. Only tracks of charged particles with reconstructed transverse momentum larger than $2 \text{ GeV}/c$ have been used. A table that translates the arbitrary run numbers used in this plot into ALICE ESD run numbers is given in the appendix B.

feature, seen in the spectrum obtained with TRD and TPC (fig. 10.5. A crosscheck with fig. 9.1 holds.). The transition of the small deuteron peak to a power law continuum is seen at $2.2 \text{ GeV}/c$. The fit was chosen to start at $2.3 \text{ GeV}/c$. The fit ends at $4.5 \text{ GeV}/c$, where fluctuations of the efficiency due to limited statistics begin and where hadron contamination is expected to start, when no TRD PID is used.

Several investigations on how to improve the efficiency comparison between data and Monte Carlo (and to reduce the differences between the five and six tracklet measurements that are present in results shown later) have been made. A natural crosscheck is to plot the ratio between the number of TRD tracklets per track in data and in Monte Carlo (fig. 10.6). Data from tracks of all charged particles with a reconstructed transverse momentum larger than $2 \text{ GeV}/c$ has been used for this purpose.

The data for this crosscheck is obtained as follows: For each data and Monte Carlo simulation run, bin number n of a histogram was incremented by one, for each track with n tracklets in the TRD. Normalising the histograms to the number of entries and dividing e.g. the bin content of bin five of the histograms from data and Monte Carlo yields the yellow circles of fig. 10.6. If the Monte Carlo representation of the TRD data runs is precise, the ratio is expected to be close to unity for all numbers of tracklets. However, less (more) tracks with six tracklets (with four, three, two and one tracklets) are seen in data when compared to Monte Carlo. If the fraction of tracks with six tracklets is higher in Monte Carlo than in data, due

to normalisation this tendency must be reversed for at least one of the other cases. Run number 10 and 22 show different behavior from the other runs. The behavior of the ratio in fig. 10.6 was studied, considering the following special cases:

- Cut $|\eta| < 0.5$,
- cut for $p_T > 5 \text{ GeV}/c$,
- use only one single TRD supermodule with all chambers working (for all of the following investigations),
- count only electron tracks identified with the TPC ($-0.5\sigma_{\text{TPC-dE/dx}} < \text{dE/dx} < 3\sigma_{\text{TPC-dE/dx}}$),
- count only V0 electron tracks,
- count only V0 electron tracks that in addition have been as electrons identified with the TPC and
- apply a cut to accept only tracks, for which the TRD track has
 - $\chi^2/\text{ndf} < 2$,
 - at least 17 clusters per TRD tracklet. (A signal from a single track can induce a charge on several pads on the read out plane at once. Pads that belong to the same track are referred to as a cluster.)

No improvement was seen for any of these investigations. Notable is, that the cut requiring at least 17 clusters per tracklet increases the spread of the ratio further to values ranging from 0.7 for six tracklets and 1.9 for two and four tracklets.

Detector alignment was not carried out for all TRD super modules that are used. It is possible that the discrepancy between data and Monte Carlo simulation that is seen in this study is reduced, when proper alignment data is implemented for all super modules.

Despite the lack of understanding of this feature, it was decided that correcting for efficiency using Monte Carlo is valid. The difference of 10% that is seen between the five and six tracklet case in fig. 10.6 is used later as estimator for the systematic uncertainty of TRD tracking.

Crosschecks were made (and are mentioned in the text where appropriate) for which the efficiency correction was done with a fit to the efficiency obtained from V0 data, using the function shown in equation 10.1. When the smooth curve of the fit is used for efficiency correction, the result fluctuates only due to limited statistics of the sample that is corrected and is not influenced additionally by the statistics of the Monte Carlo simulation.

10.3. Monte Carlo efficiency correction

The agreement in the comparison of the efficiency calculated from V0 data and Monte Carlo (compare fig. 10.3 and 10.4) allows for efficiency correction via Monte Carlo. The following results are shown in two separate sections: The efficiency corrected spectrum that is obtained when the TRD is used for particle identification is preceded by results obtained when only TRD tracking cuts, but no TRD PID is applied. In this way, the influence of the TRD particle identification properties on the spectrum can be viewed separately from its tracking efficiency.

10.3.1. Efficiency correction with only TRD tracking enabled

The signal-enhanced MC sample LHC13d3 is used for the Monte Carlo efficiency correction. The raw spectrum of inclusive electrons, together with the efficiency corrected spectrum and the efficiency from the Monte Carlo correction is shown in fig. 10.7 (fig. 10.8) for the five (six) tracklet case.

The structures at low transverse momentum are again due to contaminations of misidentified electrons (compare fig. 9.1). The five tracklet measurement shows some structure at $6 \text{ GeV}/c$ that is not present for the six tracklet case. Apart from this structure, the efficiency reaches a plateau at about $3 \text{ GeV}/c$ ($5 \text{ GeV}/c$) for the five (six) tracklet measurement. The p_T range for which the efficiency rises is broader for the six tracklet case, as a higher transverse momentum is needed for tracks to have a trajectory straight enough to pass through all layers. For p_T lower than $2.3 \text{ GeV}/c$ kaon, proton and deuteron contaminations are present in the spectrum, due to the lack of use of the TOF (compare fig. 10.5). At $p_T > 4.5 \text{ GeV}/c$ hadron contamination becomes relevant for the TPC-TRD analysis, as the TRD is only used for tracking here.

If instead of the signal-enhanced Monte Carlo simulation the minimum bias Monte Carlo sample is used for efficiency correction, the efficiency shows unexpected structure. A peak present between $5 \text{ GeV}/c$ and $6 \text{ GeV}/c$ in the efficiency of the six tracklet measurement can be reduced a little (but is still present) when the fit from equation 10.1 to the V0 efficiency (data) is used to correct for the TRD tracking efficiency instead of Monte Carlo, indicating that the peak structure originates from statistical fluctuations in the minimum bias data. The peak structure is not seen when using the signal-enhanced Monte Carlo sample. Therefore it is assumed that it is an artifact that can be attributed to limited statistics of the minimum bias MC sample and the signal-enhanced Monte Carlo simulation is used for all efficiency corrections.

The efficiency corrected TPC-TRD spectrum is compared with the spectrum obtained by the TPC-TOF analysis [19] (five tracklets case in fig. 10.9, six tracklet case in fig. 10.10). Uncorrelated errors were assumed for computing the ratio. For the five tracklet case statistics above $8 \text{ GeV}/c$ is sparse (compare fig. 10.7). Therefore the corresponding region is not shown. A constant fit to the ratio of

the two spectra yields 1.04 ± 0.03 (1.11 ± 0.03) for the five (six) tracklet case. As the TRD is only used for tracking at this stage, hadron contamination is relevant for p_T values larger than $4.5 \text{ GeV}/c$ and a comparison is not meaningful for higher transverse momenta. Hadron contamination is subtracted in the TPC-TOF analysis. Therefore the fit was done in the range from $2.3 \text{ GeV}/c$ to $4.5 \text{ GeV}/c$ where both spectra are expected to be comparable.

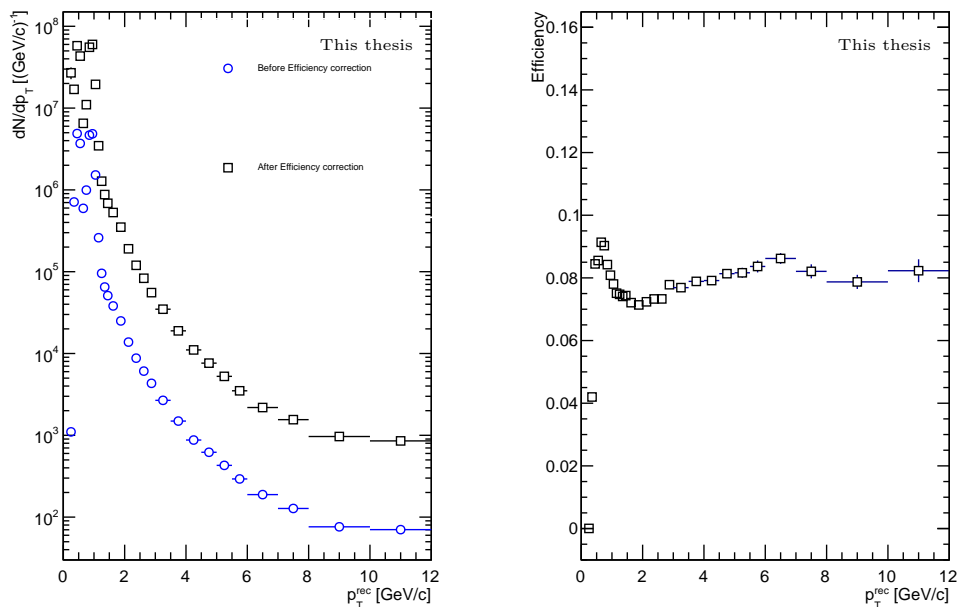


Figure 10.7.: Left: Raw and efficiency corrected inclusive electron spectrum with exactly five TRD tracklets (using the TRD for tracking only). Right: Corresponding total efficiency and acceptance of ITS, TPC and TRD with all tracking cuts applied (excluding the TPC PID efficiency of 69%).

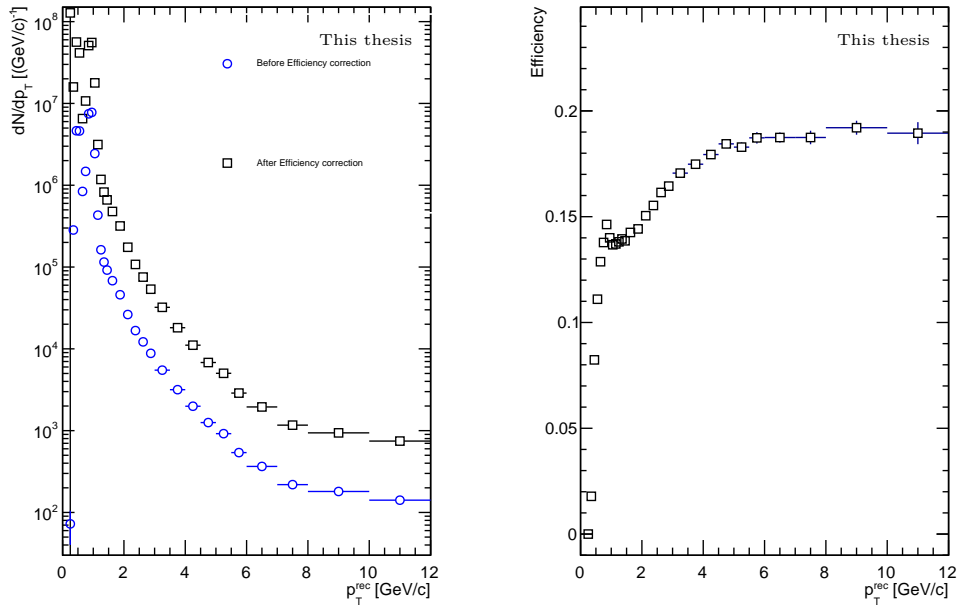


Figure 10.8.: Six tracklet case of fig. 10.7

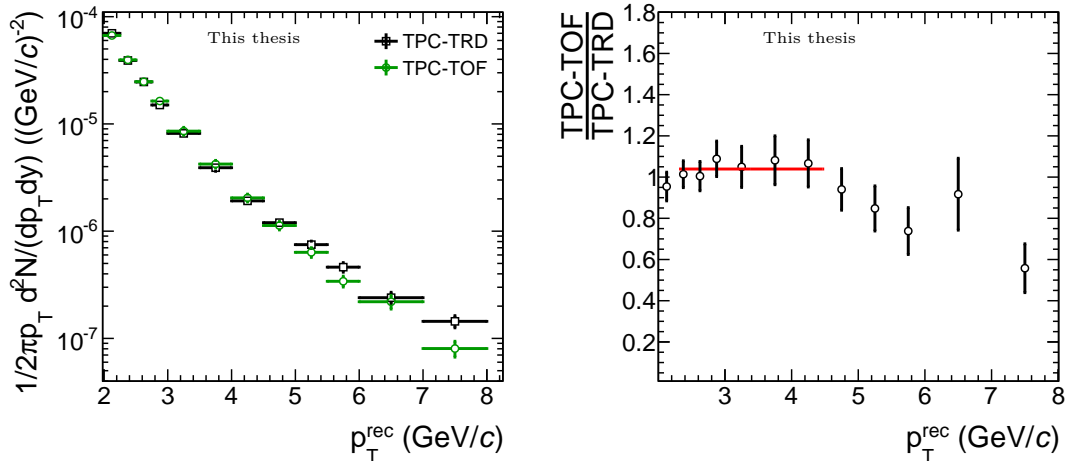


Figure 10.9.: Left: Comparison of the efficiency corrected inclusive spectrum for five TRD tracklets (using the TRD for tracking only) and the TPC-TOF analysis. As statistics above 8 GeV/c is low (compare fig. 10.7), this region is not shown for the five tracklet case. At $p_T > 4.5$ GeV/c hadron contamination becomes relevant for the TPC-TRD analysis. Hadron contamination is subtracted in the TPC-TOF analysis. Right: Ratio of both spectra. A fit in the range 2.3 GeV/c to 4.5 GeV/c yields 1.04 ± 0.03 .

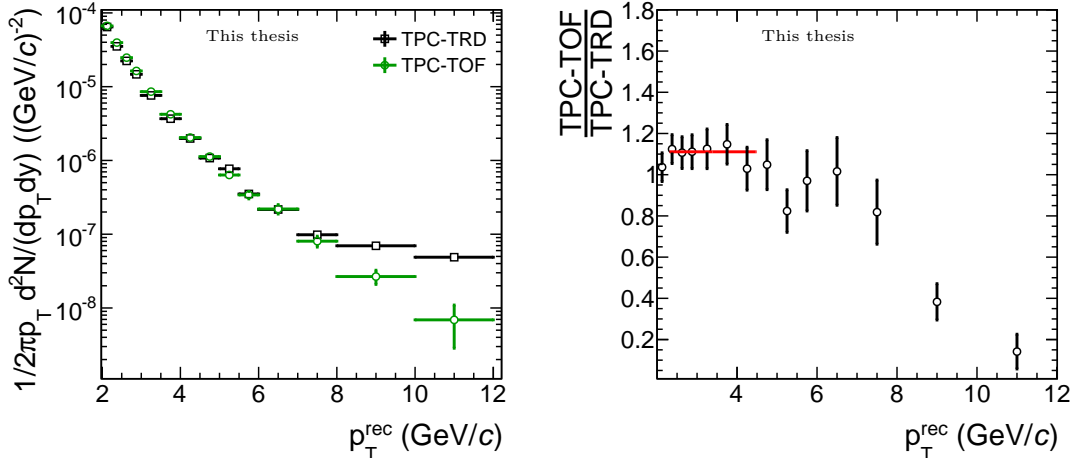


Figure 10.10.: Six tracklet case of fig. 10.9. The fit yields 1.11 ± 0.03 .

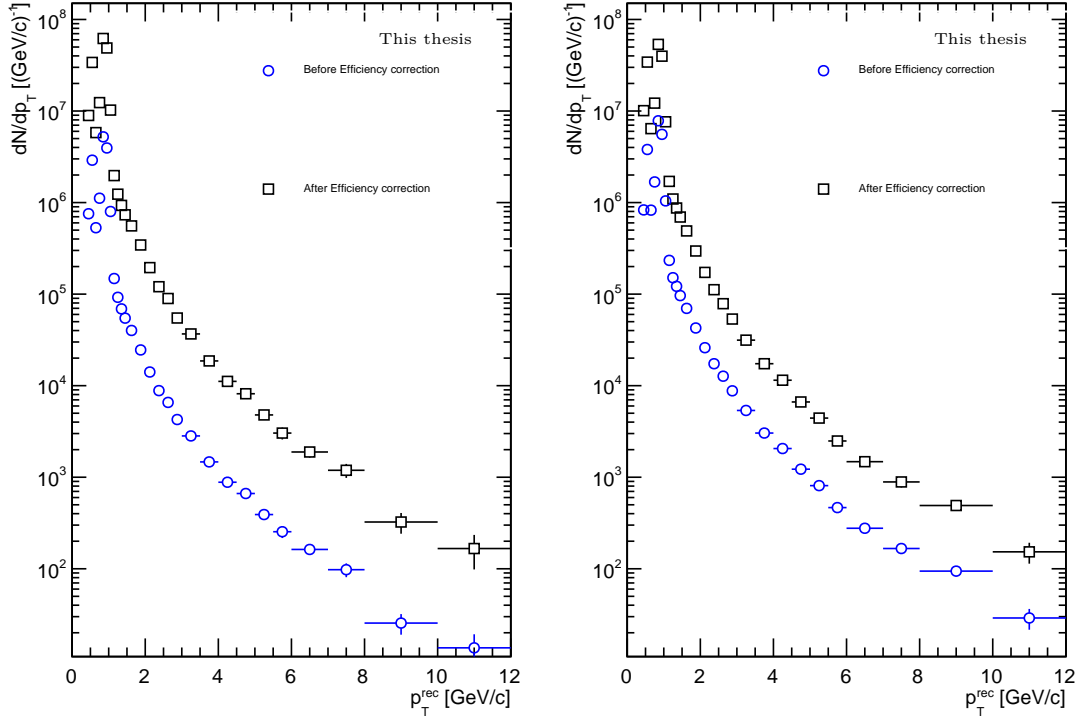
10.3.2. Efficiency with TRD tracking and TRD particle identification

The TRD particle identification cuts have visible influence on the shape of the spectrum (fig. 10.11). The number of misidentified hadrons is reduced significantly by TRD PID (as detailed in chapter 9) and thus the number of electron candidates for transverse momenta larger than 6 GeV/c has decreased drastically, compared to using the TRD for tracking only (section 10.3.1). The comparison between the TPC-TOF and the TPC-TRD analysis (fig. 10.12 and 10.13 for five and six tracklets respectively) results in a better match with TRD PID applied than it does without, for both the five and six tracklet case. Uncorrelated errors were assumed for computing the ratio.

Additional to the hadron rejection due to TRD PID, the remaining hadron contamination after TRD PID has been subtracted in the spectrum of the TPC-TRD analysis, using the description of hadron contamination shown in fig. 9.3. Thus, better agreement for transverse momenta of 4.5 GeV/c is achieved when compared to the results shown in section 10.3.1, as hadron contamination is subtracted for both analyses. However, the behavior of hadron contamination at transverse momenta larger than 6 GeV/c is not known in detail for the TPC-TOF analysis and could only be estimated [23]. For the five tracklet case, statistics above 8 GeV/c is low (compare fig. 10.7). Therefore the corresponding region is not shown.

The ratio between the TPC-TOF and TPC-TRD spectra of the five tracklet measurement is compatible with unity within the statistical uncertainties. A constant fit in the range 2.3 GeV/c to 4.5 GeV/c yields 1.01 ± 0.03 . The fit to the ratio of the six tracklet measurement between the TPC-TOF and TPC-TRD analysis yields 1.09 ± 0.04 . The ratio differs a little more than two standard deviations from unity. Additionally the ratio shows several rising features (centered at 3.3 GeV/c and

6 GeV/c) that could resemble an underlying systematic problem. These features are present but significantly less pronounced when efficiency correction is done, using the fit to the efficiency obtained from V0 data (equation 10.1) as well as when only TRD tracking is requested (fig. 10.8). The former indicates limited statistics as a possible reason.



(a) Five tracklet case.

(b) Six tracklet case.

Figure 10.11.: Raw spectrum of inclusive electrons and efficiency corrected spectrum of inclusive electrons with applied TRD PID. Hadron contamination has been subtracted in these spectra. The signal-enhanced Monte Carlo simulation is used for correction.

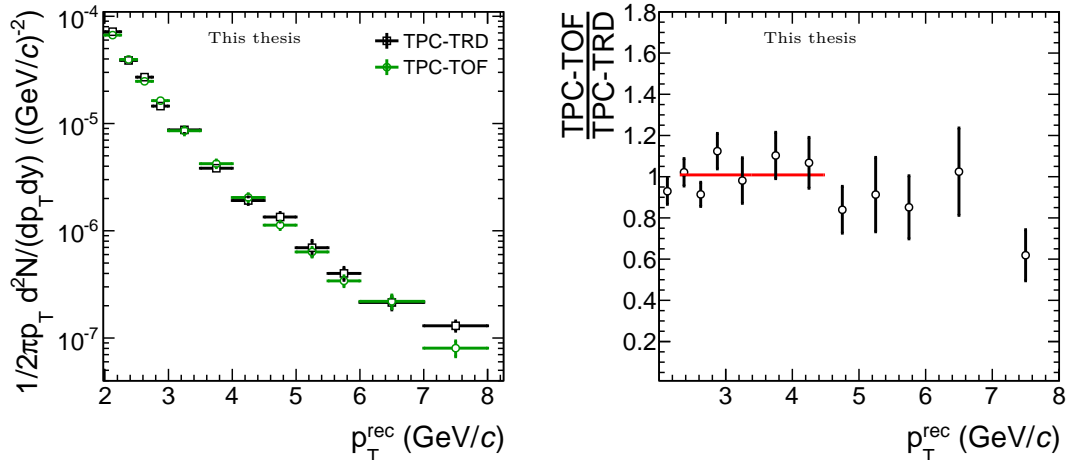


Figure 10.12.: Left: Comparison of the efficiency corrected inclusive spectrum of the TPC-TOF analysis and the TPC-TRD analysis with five TRD tracklets and applied TRD PID. Right: Ratio of both spectra. A constant fit in the range 2.3 GeV/c to 4.5 GeV/c yields 1.01 ± 0.03 .

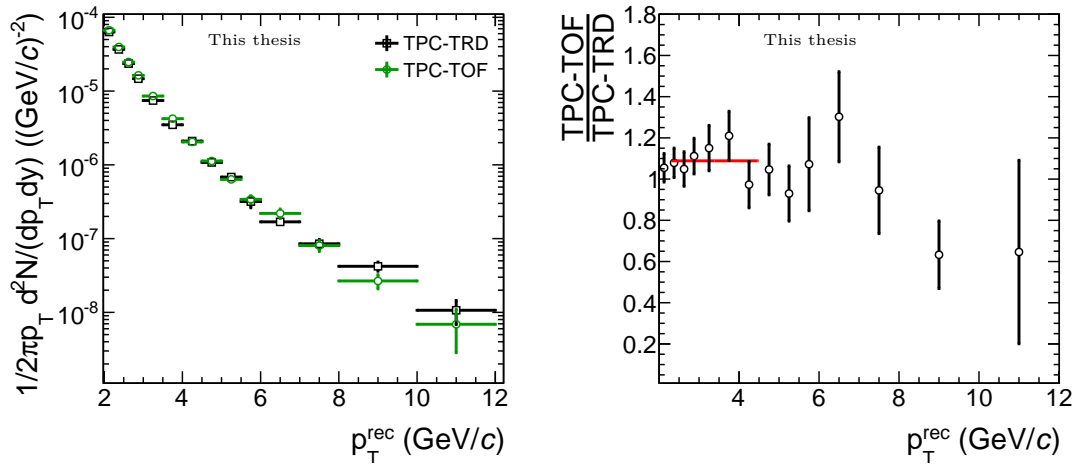


Figure 10.13.: Six tracklet case of fig. 10.12. The fit yields 1.09 ± 0.04 .

11. Estimation of systematic uncertainties

As the contribution from background electrons is carried out by statistical subtraction of a cocktail of background electrons (that is based on the measured π^0 spectrum, which is the dominant background source), it makes sense that systematic uncertainties are estimated separately for the cocktail and the inclusive spectrum. Their uncertainties are combined after background subtraction by summation in quadrature.

As most of the PID and tracking cuts used are the same as described in the analysis note of the TPC-TOF analysis [19], most of the systematic uncertainty estimations can be adopted, the prominent exception being the absence of TOF and new systematic uncertainties introduced by the use of the TRD for tracking and PID. Systematic uncertainties of the TRD are threefold:

Systematics due to the imperfect Monte Carlo simulation and TRD matching efficiency are estimated with the comparison of TRD tracking efficiency obtained with V0 data. The deviation from unity of the ratio between data and Monte Carlo efficiency obtained in this way (fit value in bottom plot in fig. 10.3) is the estimator for the systematic uncertainty. The larger of the two values obtained for the five and six tracklet case is used as an estimate. The uncertainty from tracking is estimated by two methods. The first method consists of comparing the efficiency corrected spectrum of the five tracklet case with the six tracklet spectrum (fig. 11.1) for which a constant fit in the transverse momentum range of $2.3 \text{ GeV}/c$ to $6 \text{ GeV}/c$ yields 0.92 ± 0.02 . The method consists of using the difference of 10% that is seen between the five and six tracklet case for the number of TRD tracklets per track in fig. 10.6. As the latter is the larger contribution of the two, it was decided that this should be used as an estimate for the systematic uncertainty associated with TRD tracking.

An upper limit of TRD PID systematics is obtained by:

- The size of the uncertainty of a fit to the resulting electron efficiency of the PID cut.
- The variation of the fit result, using only V0 electrons.

These results are compared with a variation of the TRD electron efficiency cut and it is found that the results of the different approaches agree within a variation of 3%.

Source	Systematic uncertainty [%]
ITS clusters	2
TPC clusters	2
TPC PID clusters	2
DCA	negligible
ITS-TPC matching	2.5
TPC PID ($p_T < 6 \text{ GeV}/c$)	5
η and charge	4
MC sample and unfolding	3
TRD matching and MC simulation	5.4
TRD tracking	10
TRD PID	3
total	14

Table 11.1.: Systematic uncertainties for the inclusive electron spectrum, taken from the TPC-TOF analysis [19] (except for the uncertainties associated with the TRD). The individual contributions are assumed to be uncorrelated. The total systematic uncertainty is thus obtained by summation in quadrature. A crosscheck with and without the signal-enhanced Monte Carlo simulation was made in order to verify that the systematic uncertainty associated with the Monte Carlo simulation and the unfolding process still holds.

An overview of all contributions to the systematic uncertainty is given in table 11.1. The individual contributions are assumed to be uncorrelated and thus the total systematic uncertainty obtained by summation in quadrature.

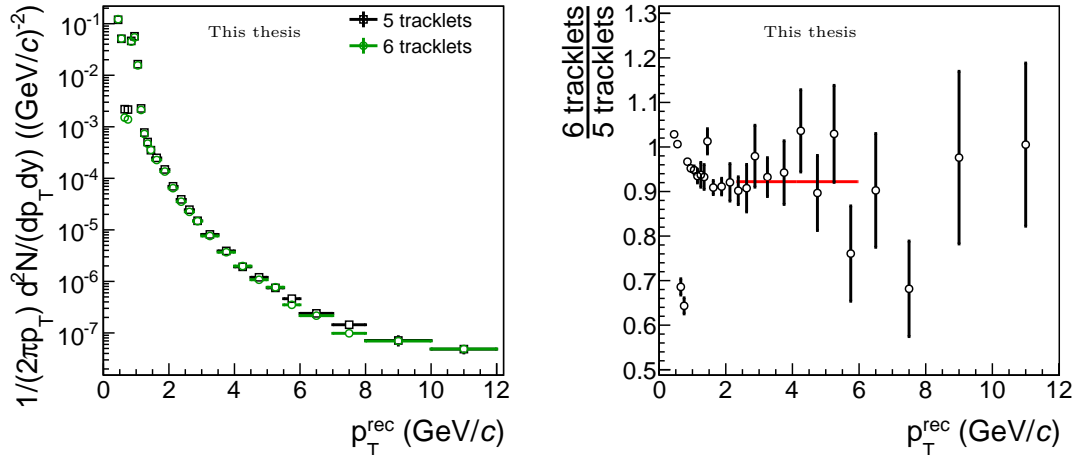


Figure 11.1.: Comparison of the five and six tracklet efficiency corrected inclusive electron spectrum for which only TRD tracking cuts are applied. The signal-enhanced Monte Carlo sample was used for efficiency correction. A constant fit in the transverse momentum range of 2.3 GeV/c to 6 GeV/c yields 0.92 ± 0.02 .

12. Results: HFE spectrum and R_{pPb}

The efficiency corrected inclusive electron spectrum as shown in section 10.3.2 contains electrons not only from heavy-flavour hadron decays, but also from various background sources [19]:

- Dalitz decays of light neutral mesons (π^0, η, η'),
- photon conversion,
- dielectron decays of light vector mesons (ρ, ω, ϕ),
- dielectron decays of heavy quarkonia ($J/\psi, \Upsilon$, etc),
- and weak kaon decays (K_{e3}).

Background electrons are statistically subtracted from the efficiency corrected inclusive electron spectrum with the use of a cocktail of background electrons, as described in the analysis note of the TOF and TPC HFE analysis [19].

The background is dominated by decays of the neutral pion. The cocktail input is based on the measured spectrum of charged pions, from which the π^0 spectrum is obtained, assuming that the invariant yields behave as $\pi^0 = (\pi^+ + \pi^-)/2$. From the measured spectrum of pions, the contributions of other mesons to the cocktail is obtained via m_T -scaling and the amount of background electrons due to photon conversion and K_{e3} decays can be calculated [19].

The cocktail is made up of electrons that are either obtained directly from the efficiency corrected spectrum of pions or derived with the efficiency corrected spectrum of pions as input so the cocktail of background electrons itself contains efficiency corrected electron yields and therefore has to be subtracted after the efficiency correction is applied. The systematic uncertainty of the cocktail is approximately a constant of 8.5% as function of p_T [19].

The obtained spectrum of electrons from semi-leptonic heavy-flavour hadron decays in p-Pb collisions at $\sqrt{s_{NN}} = 5.02$ TeV is shown in fig. 12.1 and 12.2 for the five and six tracklet measurement respectively, together with a comparison of the results obtained by an analysis using TPC and EMCal. In contrast to the TPC-EMCal analysis, a comparison with the TPC-TOF result above 6 GeV/ c is insignificant due to increasing hadron contamination.

The TPC-TRD result was re-binned for the calculation of the ratio plots fig. 12.1b and 12.2b. Results for p_T values larger than 8 GeV/ c lack statistics for a meaningful

comparison in case of the five tracklet measurement (compare fig. 10.11a) and thus are not shown in the plots.

Up to a transverse momentum of 8 GeV/ c , the spectrum measured with the TRD has a tendency to fall less steep than the TPC-EMCal result. The points measured with TPC-TRD are in most cases higher than the TPC-EMCal counterparts. The five and six tracklet measurements show deviation from one another. The six tracklet measurement, which has higher statistics, is closer to the TPC-EMCal result. Respecting the fairly large systematic uncertainty of the ratio (uncorrelated errors were assumed), both, the five and six tracklet spectrum can be compatible with the TPC-EMCal result.

For a proper interpretation of R_{AA} results from Pb-Pb collision data, a further reference to identify possible non-QGP nuclear effects is needed. This reference is provided by the nuclear modification factor R_{pPb} , measured in proton-lead collisions, which is defined as:

$$R_{pPb} = \frac{dN^{pPb}/dp_T}{\langle T_{pPb} \rangle d\sigma^{pp}/dp_T} , \quad (12.1)$$

with the differential yield dN^{pPb}/dp_T in p-Pb collisions, the differential cross section $d\sigma^{pp}/dp_T$ at $\sqrt{s} = 5.02$ TeV in pp collisions (which was scaled down to $\sqrt{s} = 5.02$ TeV from measured data at $\sqrt{s} = 7$ TeV) and the nuclear overlap function $\langle T_{pPb} \rangle$, which is calculated to be $\langle T_{pPb} \rangle = 0.0983 \text{ mb}^{-1} \pm 0.0035 \text{ mb}^{-1}$ [19]. The systematic uncertainty of the pp-reference is between 20 % and 30 %, increasing for larger p_T . The so computed R_{pPb} is shown in fig. 12.3 together with a comparison to the TPC-EMCal result. The six tracklet measurement yields a systematically lower R_{pPb} and is in better agreement with the TPC-EMCal result compared with the result for five TRD tracklets.

Compared to the six tracklet measurement, the five tracklet case tends to result in higher R_{pPb} values. However, no significant deviation from unity is observed. Especially the six tracklet measurement and to a lesser extend also the five tracklet case are compatible with the hypothesis of a R_{pPb} equal to one. Fluctuation of data points is a necessary feature of statistics. With more data, a clearer picture can be obtained.

The systematic uncertainty of TPC particle identification, was estimated for the TPC-TOF analysis and with respect to transverse momenta smaller than 6 GeV/ c . The systematic uncertainty of the cocktail was only checked below 10 GeV/ c and the TRD hadron contamination for momenta larger than 10 GeV/ c is based on an extrapolation (compare section 9, page 50). These factors can explain some of the discrepancy that is seen. Additionally, the TPC signal has a ϕ dependency that is usually quantified with its integrated contribution over all ϕ values and thus valid only if an analysis uses the full azimuth of the TPC. As the TRD was not installed in full azimuthal coverage during data taking, distribution of the TRD in ϕ might influence the systematic uncertainty value of TPC PID (compare tab. 11.1) in which this effect is included.

Because of the differences that are seen between the measurements with five and six TRD tracklets, we omitted a combination into a single result.

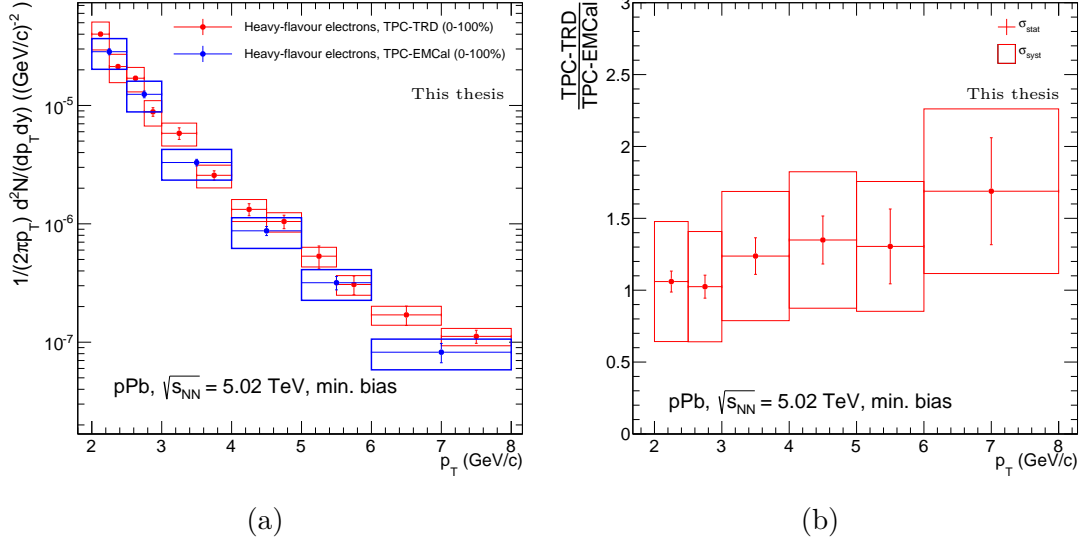


Figure 12.1.: (a) The p_T spectrum of electrons from heavy-flavour hadron decays identified with TPC and TRD (five tracklets) in comparison with the result of TPC-EMCal. (b) The ratio of the two spectra (the TPC-TRD spectrum is rebinned to fit the TPC-EMCal result).

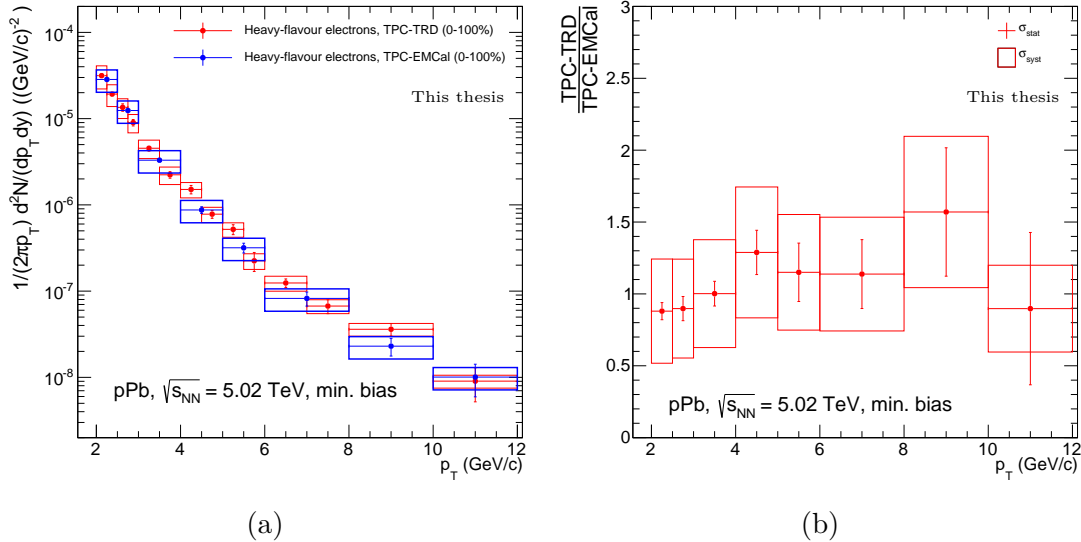


Figure 12.2.: Six tracklet case of fig. 12.1.

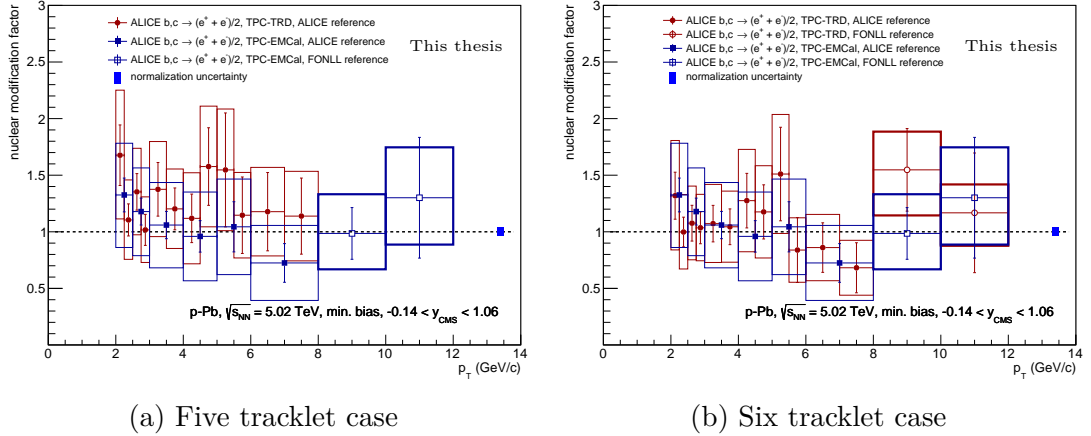


Figure 12.3.: Resulting R_{pPb} in comparison with the TPC-EMCal analysis.

12.1. Summary and prospects

The TRD has been used to conduct an analysis of electrons from semi-leptonic heavy-flavour hadron decays in p-Pb collisions at $\sqrt{s_{NN}} = 5.02$ TeV. In the course of the analysis, the implementation of the TRD in the Monte Carlo runs anchored to the data taking periods LHC13b and LHC13c has been refined by identification of misrepresented chambers. Using a data driven method, it could be confirmed that the efficiency correction with the Monte Carlo simulation is valid. The systematic uncertainties associated with TRD tracking, track matching, PID and its representation in the Monte Carlo simulation have been estimated to be 14%.

The resulting electron spectrum is compatible with the TPC-TOF analysis and the analysis done with TPC and EMCal within uncertainties. Yet, the TPC-TRD spectrum yields higher data points than the TPC-EMCal result for the majority of p_T intervals. There is a difference seen between the results with five and six TRD tracklets. Therefore it was chosen to omit a combination of both measurements into a single result.

The resulting R_{pPb} shows no significant suppression or enhancement effects. However, the R_{pPb} measured with five TRD tracklets has a tendency to be higher than the TPC-EMCal result and shows only points above unity. The results of the TPC-TOF analysis have been extended to the range from 6 GeV/c to 12 GeV/c with the use of the TRD.

For future analyses, a better understanding of the TRD tracking behaviour and its representation in the Monte Carlo simulation is needed. An important step towards this goal is to have proper alignment of all installed TRD super modules. With increased statistics, a clearer picture of the current results as well as analysis at higher transverse momenta becomes possible and more data will allow a viable measurement with five TRD tracklets for p_T values larger than 8 GeV/c. More data of heavy-flavour hadron decay events can be obtained, if the ALICE TRD is used for triggering on high transverse momentum events, providing an enriched

data sample with a clear benefit over the currently used minimum bias trigger. The uncertainty that is associated with the hadron contamination and the subsequent subtraction of hadrons is an influence, which has not been taken in to account yet. Additional room for improvements can be made by varying the TRD particle identification cut in order to find the best possible compromise between hadron contamination and electron yield. Furthermore, the influence of the TPC PID cut on the hadron contamination is an aspect of the analysis that needs to be optimized for high momentum measurement.

Appendix

A. Miscellaneous practical information for setting up the chromatograph

A.1. Enable XML file export of Agilent ChemStation

The DIM Server relies on the XML files that Agilent ChemStation can produce. To enable XML export, open `C:\Windows\ChemStation.ini` and under [PCS] add the line “**XMLEnableExport=1**”. This functionality is not enabled by default after a fresh installation.

A.2. Pre-run parameters - auxiliary commands

SRA ProChem is used to operate the chromatograph together with the stream selector. By default, ProChem will not close streams after sampling is finished and the currently selected stream on the stream selector is directly connected with the exhaust after the flow meter (2.3). SRA ProChem offers “Auxiliary commands” to prevent this. In ProChem, a file with auxiliary commands can be created in `Sequence >> Auxiliary commands`.

Using the commands

1. Select the current stream
2. Start GC
3. Select the default stream

in the above order ensures that the stream is closed after sampling (and thus no gas is wasted). Starting the Chromatograph before the default stream is selected, prevents air from leaking into the sampling loop. Sampling time (the time between step 1 and 2) is set to last for 20s. Between step 2 and 3 pass two seconds. In order to use the auxiliary commands for each measurement, specify the path to the event file under `Process >> Start >> Event file`.

A.3. Setting up Visual Studio to compile a DIM server

To successfully compile code in a new Visual Studio project that uses the DIM library, the following steps are necessary:

- Get DIM for Windows from http://dim.web.cern.ch/dim/dim_wnt.html (I used http://dim.web.cern.ch/dim/dim_v20r7.zip) and extract it.
- In Visual Studio create a new Project of "Application Type" "Console application". Check "Additional options" "Empty project".
- In Visual Studio, open the project's properties via **Project** » **'projectname' Properties** » **Configuration Properties** » **VC++ Directories** » **General** » **Include Directories** and add the path to `dim_xxxx\dim` that you downloaded and extracted before (e.g. `C:\dim_v20r7\dim`).
- In the same menu, add to **General** » **Library Directories** the path to `dim_xxxx\bin32`.
- Still in the project's properties, go to **Configuration Properties** » **Linker/Input**, edit **Additional Dependencies** and type there "dim.lib".

With this, compiling is possible.

To execute the resulting application, "dim.dll" from `dim_xxxx\bin32` must reside in the same folder as the application.

A.4. Miscellaneous hints

- If a new method is created or after installing the GC software on a new machine, the TCD needs to be selected as the signal source in **Method** » **Edit Entire Method...** » **Instrument/Acquisition** » **Signals** » **Signal Source**. There is a drop-down menu that can be accessed via click on the small arrow.
- Agilent ChemStation crashes frequently, if for a method in the menu **Method** » **Edit Entire Method...** » **Data analysis** » **OK** » **OK** » **OK** » **Report Settings** » **Destination** the option "Screen" is enabled. Be sure to disable this. If disabled, the measurement results are not shown on the screen by default after a method is completed.

B. Tables

#run	ALICE ESD run number	$\frac{\text{event count of run}}{\text{total event count}}$ [%]
0	195344	0.1
1	195351	0.4
2	195389	0.8
3	195391	0.9
4	195478	0.2
5	195479	6.8
6	195480	1.1
7	195481	0.2
8	195482	2.0
9	195483	11.9
10	195529	0.3
11	195531	27.0
12	195566	3.9
13	195567	4.1
14	195568	12.0
15	195592	0.7
16	195593	6.9
17	195596	0.9
18	195633	1.3
19	195635	1.9
20	195644	9.1
21	195673	5.1
22	195675	0.1
23	195677	2.3

Table B.1.: Translation of the arbitrary run numbers used in fig. 10.6 into ALICE ESD run numbers.

C. Lists

List of Figures

1.1.	A schematic view of ALICE [1]. The detectors that are relevant for this thesis have been labeled.	3
1.2.	A schematic view of the ALICE TPC [2].	3
1.3.	Cross section through a TRD detector module [5]. The dimensions are given in mm, e.g the drift volume has a depth of 37 mm. Particles pass from bottom to top.	4
1.4.	Mean pulse height of the signal of an electron and pion track induced on the pad plane, as a function of drift time [5].	5
1.5.	ALICE cross section, indicating the installation status of the TRD during the 2013 data runs.	6
1.6.	Locations of the various units of the TRD gas system [5].	8
1.7.	General layout of the TRD gas system [5]. (The position of the buffer unit is not in the surface gas building, as depicted here, but on the plug.)	9
2.1.	The Agilent 7890A gas chromatograph (a) with the stream selector (b) and switching valves (c) by SRA.	15
2.2.	A chromatogram for the TPC gas as produced by Agilent Chem-Station. Vertical numbers denote the retention time in minutes of any peak that the software found. Magenta parts of the time axis illustrate the region that was used for integration of peak area. The peak at a retention time of 3 minutes corresponds to CO ₂ , the peak at 5.9 minutes to argon. At 5.5 minutes a peak of neon with a relative area of 0.009% (uncalibrated) is present as a remainder from the previously used gas mixture in the TPC. The peak at 2.8 minutes is a measurement artifact that is produced when the switching valve V2 is actuated. The peak 7.5 minutes is of unknown origin.	16
2.3.	Schematic, depicting the switching valve layout of the gas chromatograph. The compounds being analysed enter the system at the stream selector. The switching valves V1 and V2 have two states (on/off). The dashed (thin) lines show the interconnections that the valves use in the “on”(“off”) state. For example, if V1 is on and V2 off, the carrier gas pushes the content of the sampling loop through Column 1 and 2 (C1 and C2) to the TCD and the outlet of the Stream Selector is directly exhausted through a flow meter.	17

2.4.	Analysis of the TRD gas using two sampling loops of different size. The three peaks from left to right correspond to air, CO ₂ and xenon. The smaller sampling volume (b) visibly improves separation of Xenon and CO ₂ . The air that is present in this measurements is contamination in the tubing that connects the chromatograph and the TRD calibration gas tank and presumably entered the system during the installation of this connection.	19
2.5.	Schematic drawing of the TCD [14]. From the bottom upwards, the effluent of the columns is mixed with the make-up gas before it reaches the chamber where the filament (zigzag structure) is located. A switching valve (dashed box) can be set to push the column effluent away from (or towards) the filament as shown in the left (right) diagram, such that reference gas (or sampling gas from the columns) flows over the filament. The filament is heated and when it is in alternating contact with gases of different thermal conductivity, its temperature (and thus its resistance) changes. The resistance change is measured in a wheatstone bridge circuit that produces the TCD output signal. The switching valve is set to operate at 5Hz.	20
2.6.	Analysis of the TPC gas, using only column 1 for separation.	23
2.7.	Analysis of the TRD gas, using only column 1 for separation.	24
2.8.	Histograms, showing the distributions of the measured CO ₂ (a) and argon (b) fraction in the TPC gas that were obtained over the period of one month of continuous measurements.	26
3.1.	Illustration of the data flow from the gas chromatograph to the detector control systems of the TPC and TRD.	29
3.2.	The WinCC panel of the gas chromatograph in the TPC detector control system. The central feature is a trending plot that shows the gas composition as a function of time. Blue points show the fraction of argon, purple points the fraction of CO ₂ in the gas mixture.	30
9.1.	Energy loss of charged particles as measured by the TPC as a function of momentum. The expectation value of the electron hypothesis is shifted to zero and is normalised to a standard deviation of the energy loss signal. For these plots, only tracks with six TRD tracklets have been used. Results with (b) and without (a) TRD PID reveal the TRD hadron rejection capabilities. TRD PID is not applied on tracks with momenta lower than 0.5 GeV/c and corresponding tracks are not shown in (b). The black horizontal lines show the PID cut of $-0.5\sigma_{\text{TPC-dE/dx}} < \text{dE/dx} < 3\sigma_{\text{TPC-dE/dx}}$ applied to the TPC signal.	51

9.2.	The number of particle tracks in the momentum range from 2.6 GeV/ c to 10 GeV/ c as a function of TPC dE/dx subtracted by the electron hypothesis in units of the standard deviation shows the hadron rejection capability of the TRD: Green diamonds show the number of particles using TPC PID only. In blue circles, the same data is shown with applied TRD PID cut for an electron efficiency of 53.3%, that is used in this analysis. The number of electrons (peak centered around zero) is reduced to 53.3%, whereas the number of pions is reduced dramatically to only 0.02%, resulting in a much lower pion contamination of the electron candidate sample.	52
9.3.	Hadron contamination for particle momenta larger 4 GeV/ c as a function of particle momentum p for the PID cuts that are used for the TPC and TRD [23]. With applied TRD PID, there is nearly zero hadron contamination up to 6 GeV/ c instead of about 10% using the TPC only. At 10 GeV/ c , the TPC-only PID strategy yields an unusable fraction of about 80% hadrons in the electron candidate sample that is reduced to below 15% with TRD PID and six TRD tracklets. The hadron contamination for momenta larger than 10 GeV/ c is extrapolated from the data at lower p values.	53
10.1.	Number of entries in layer 3 of the TRD as a function of η and ϕ in data run 195531 (ALICE internal convention for run identification). Only tracks of positive charge with a reconstructed transverse momentum larger than 2 GeV/ c are shown. In the two white areas centered at $\phi \approx 1.7$ and $\phi \approx 4.7$ no super modules have been installed during the 2013 LHC runs (compare fig. 1.5).	57
10.2.	Difference of η - ϕ maps obtained from data and from the Monte Carlo simulation for the same tracks that were used for fig. 10.1. The three chambers that show abnormal deviation from zero (centered at $\eta = 0.7$, and $\phi = 2.5, 3.2$ and 6) were removed for the analysis and are also mapped out in fig. 10.1.	57
10.3.	Top: Comparison of TRD tracking efficiency using V0 electron data and the minimum bias Monte Carlo simulation with exactly five TRD tracklets. Bottom: The ratio of the two distributions. A constant fit from 2.3 to 4.5 GeV/ c yields 0.946 ± 0.068	60
10.4.	Six tracklet case of fig. 10.3. A constant fit from 2.3 to 4.5 GeV/ c yields 1.000 ± 0.045	60

10.5. Zoom into the low end of the inclusive electron spectrum, measured with TPC-TRD, in comparison with the TOF-TPC result. Since the time of flight detector is not used in the TRD analysis, the kaons, protons (two leftmost points) and deuterons (slight excess in the range $1.5 \text{ GeV}/c$ to $2.2 \text{ GeV}/c$) that are present in the low p_T range of the spectrum can not be distinguished from electrons and contaminate the spectrum with peak structures. The fit that is used later for comparison with the TPC-TOF analysis starts at $2.3 \text{ GeV}/c$, because the high p_T end of the deuteron feature is absent from this point onwards. A crosscheck with fig. 9.1 holds. The spectrum of the TPC-TOF analysis is plotted in order to identify the transition from the deuteron feature to the power law behaviour of the inclusive electron spectrum.	61
10.6. Ratio of the number of TRD tracklets per track for individual runs. Only tracks of charged particles with reconstructed transverse momentum larger than $2 \text{ GeV}/c$ have been used. A table that translates the arbitrary run numbers used in this plot into ALICE ESD run numbers is given in the appendix B.	62
10.7. Left: Raw and efficiency corrected inclusive electron spectrum with exactly five TRD tracklets (using the TRD for tracking only). Right: Corresponding total efficiency and acceptance of ITS, TPC and TRD with all tracking cuts applied (excluding the TPC PID efficiency of 69%).	65
10.8. Six tracklet case of fig. 10.7	66
10.9. Left: Comparison of the efficiency corrected inclusive spectrum for five TRD tracklets (using the TRD for tracking only) and the TPC-TOF analysis. As statistics above $8 \text{ GeV}/c$ is low (compare fig. 10.7), this region is not shown for the five tracklet case. At $p_T > 4.5 \text{ GeV}/c$ hadron contamination becomes relevant for the TPC-TRD analysis. Hadron contamination is subtracted in the TPC-TOF analysis. Right: Ratio of both spectra. A fit in the range $2.3 \text{ GeV}/c$ to $4.5 \text{ GeV}/c$ yields 1.04 ± 0.03	66
10.10 Six tracklet case of fig. 10.9. The fit yields 1.11 ± 0.03	67
10.11 Raw spectrum of inclusive electrons and efficiency corrected spectrum of inclusive electrons with applied TRD PID. Hadron contamination has been subtracted in these spectra. The signal-enhanced Monte Carlo simulation is used for correction.	68
10.12 Left: Comparison of the efficiency corrected inclusive spectrum of the TPC-TOF analysis and the TPC-TRD analysis with five TRD tracklets and applied TRD PID. Right: Ratio of both spectra. A constant fit in the range $2.3 \text{ GeV}/c$ to $4.5 \text{ GeV}/c$ yields 1.01 ± 0.03	69
10.13 Six tracklet case of fig. 10.12. The fit yields 1.09 ± 0.04	69

11.1. Comparison of the five and six tracklet efficiency corrected inclusive electron spectrum for which only TRD tracking cuts are applied. The signal-enhanced Monte Carlo sample was used for efficiency correction. A constant fit in the transverse momentum range of 2.3 GeV/ c to 6 GeV/ c yields 0.92 ± 0.02	73
12.1. (a) The p_T spectrum of electrons from heavy-flavour hadron decays identified with TPC and TRD (five tracklets) in comparison with the result of TPC-EMCal. (b) The ratio of the two spectra (the TPC-TRD spectrum is rebinned to fit the TPC-EMCal result).	77
12.2. Six tracklet case of fig. 12.1.	77
12.3. Resulting R_{pPb} in comparison with the TPC-EMCal analysis.	78

List of Tables

2.1. Connection layout of the stream selector. On the software side, there is an eleventh stream (“default stream”) that is selected in order to close an open stream.	18
8.1. Track selection cuts [19].	47
10.1. TRD chambers that are disabled in the analysis due to discrepancies that are seen between data and the Monte Carlo simulation. The contribution of the runs to the total event count can be found in the appendix B, tab. B.1.	58
11.1. Systematic uncertainties for the inclusive electron spectrum, taken from the TPC-TOF analysis [19] (except for the uncertainties associated with the TRD). The individual contributions are assumed to be uncorrelated. The total systematic uncertainty is thus obtained by summation in quadrature. A crosscheck with and without the signal-enhanced Monte Carlo simulation was made in order to verify that the systematic uncertainty associated with the Monte Carlo simulation and the unfolding process still holds.	72
B.1. Translation of the arbitrary run numbers used in fig. 10.6 into ALICE ESD run numbers.	85

Bibliography

- [1] Aamodt, K. and ALICE Collaboration, “The ALICE experiment at the CERN LHC”. In: *JINST* 3 (2008), S08002. DOI: 10.1088/1748-0221/3/08/S08002.
- [2] J. Alme et al., “The ALICE TPC, a large 3-dimensional tracking device with fast readout for ultra-high multiplicity events”. In: *Nuclear Instruments and Methods in Physics Research A* 622 (Oct. 2010), pp. 316–367. DOI: 10.1016/j.nima.2010.04.042. arXiv: 1001.1950 [physics.ins-det].
- [3] A. Andronic, S. Biagi, P. Braun-Munzinger, C. Garabatos, and G. Tsileidakis, “Drift velocity and gain in argon- and xenon-based mixtures”. In: *Nuclear Instruments and Methods in Physics Research A* 523 (May 2004), pp. 302–308. DOI: 10.1016/j.nima.2003.11.426. eprint: physics/0402044.
- [4] A. Andronic and J. P. Wessels, “Transition radiation detectors”. In: *Nuclear Instruments and Methods in Physics Research A* 666 (Feb. 2012), pp. 130–147. DOI: 10.1016/j.nima.2011.09.041. arXiv: 1111.4188 [physics.ins-det].
- [5] ALICE Collaboration, *Technical Design Report of the Transition Radiation Detector*. 2001. URL: <http://www-alice.gsi.de/trd/tdr/index.html>.
- [6] Walter Blum, Werner Riegler, and Luigi Rolandi, *Particle Detection with Drift Chambers*. Springer, 2008.
- [7] R. Veenhof, *Choosing a gas mixture for the ALICE TPC*. Internal Note/TPC, ALICE-INT-2003-29 version 1.0. May 10, 2003.
- [8] Nora Pitz, “Gas system, gas quality monitor and detector control of the ALICE Transition Radiation Detector and studies for a pre-trigger data read-out system”. PhD thesis. Goethe University Frankfurt, 2012.
- [9] Peter J. Baugh (Hrsg.), *Gaschromatographie. Eine anwenderorientierte Darstellung*. Vieweg, 1997.
- [10] *Agilent 7890A gas chromatograph*. <http://www.chem.agilent.com/Library/datasheets/Public/5989-6317EN.pdf>.
- [11] *SRA Instruments. chromatographic solutions*. <http://www.sra-instruments.com>.
- [12] *Agilent ChemStation Rev. C.01.05*. <http://www.chem.agilent.com/en-US/products-services/Software-Informatics/GC-MSD-ChemStation-Software/Pages/default.aspx>.

- [13] *SRA ProChem 2.7.4. Supervision software OpenLab Chemstation Agilent GC*. <http://www.sra-instruments.com/en/index.php?page=prochem.htm>.
- [14] Agilent Technologies, *Agilent 7890A Gas Chromatograph Advanced User Guide*. 2012.
- [15] Agilent Technologies, *Thermal Conductivity Detector Troubleshooting Tips*. URL: <http://www.chem.agilent.com/Library/Support/Documents/a16093.pdf>.
- [16] C. Gaspar and M. Donszelmann, “DIM: A distributed information management system for the DELPHI experiment at CERN”. In: (1993), pp. 156–158.
- [17] Aamodt, K. and ALICE Collaboration, “Two-pion Bose-Einstein correlations in central Pb-Pb collisions at $\sqrt{s_{NN}} = 2.76$ TeV”. In: *Phys.Lett.* B696 (2011), pp. 328–337. DOI: 10.1016/j.physletb.2010.12.053. arXiv: 1012.4035 [nucl-ex].
- [18] P. Braun-Munzinger, “Quarkonium production in ultra-relativistic nuclear collisions: Suppression versus enhancement”. In: *J.Phys.* G34 (2007), S471–478. DOI: 10.1088/0954-3899/34/8/S36. arXiv: nucl-th/0701093 [NUCL-TH].
- [19] R. Auerbeck, M. Fasel, S. Masiocchi, Y. Pachmayer, and J. Wagner, *Measurement of electrons from semi-leptonic heavy-flavour hadron decays in p-Pb collisions at $\sqrt{s_{NN}} = 5.02$ TeV*. ALICE internal note (prelim. result). Mar. 24, 2014.
- [20] Stefan Roesler, Ralph Engel, and Johannes Ranft, “The Monte Carlo event generator DPMJET-III”. In: (2000), pp. 1033–1038. arXiv: hep-ph/0012252 [hep-ph].
- [21] Xin-Nian Wang and Miklos Gyulassy, “HIJING: A Monte Carlo model for multiple jet production in p p, p A and A A collisions”. In: *Phys.Rev.* D44 (1991), pp. 3501–3516. DOI: 10.1103/PhysRevD.44.3501.
- [22] Martin Völkl, “Study of the Transverse Momentum Spectra of Semielectronic Heavy Flavor Decays in pp Collisions at $\sqrt{s} = 7$ TeV and Pb-Pb Collisions at $\sqrt{s_{NN}} = 2.76$ TeV with ALICE”. MA thesis. University of Heidelberg, 2012.
- [23] Yvonne Pachmayer, *Private communication*. Physikalisches Institut, University of Heidelberg. 2014.

Acknowledgments

I like to thank Johanna Stachel for giving me the opportunity to join her group. I owe gratitude to Kai Schweda for encouragement and guidance, for the offer to do this thesis and for the comments upon reading this work.

I am thankful to Norbert Herrmann for reading and evaluating this thesis.

I wish to express my gratitude to my supervisors Chilo Garabatos and Yvonne Pachmayer for guidance, support and explanations throughout my thesis and for providing a great working atmosphere. I thank Chilo Garabatos, for proof reading the hardware part of this thesis. For proof reading the analysis part, I wish to thank Yvonne Pachmayer, Martin Völkl and Michael Winn. Very special thanks to Michael Winn for the numerous answers that helped me in the process of understanding.

Many thanks to Cristiane Jahnke for helping me out last-minute with the FONLL pp-reference.

I thank Klaus Reygers and Kai Schweda for exciting my curiosity during your lecture that lead me to work on this thesis.

Mein besonderer Dank gilt außerdem meiner Familie, die mich während des Studiums bedingungslos Unterstützt hat.

Erklärung:

Ich versichere, dass ich diese Arbeit selbstständig verfasst habe und keine anderen als die angegebenen Quellen und Hilfsmittel benutzt habe.

Heidelberg, den 18. September 2014

.....